

# Interaction-Enabled Two- and Three-Fold Exceptional Points

Musashi Kato<sup>1,\*</sup> and Tsuneya Yoshida<sup>1,†</sup>

<sup>1</sup>*Department of Physics, Kyoto University, Kyoto 606-8502, Japan*

(Dated: February 17, 2026)

We propose a novel type of exceptional points, dubbed interaction-enabled  $n$ -fold exceptional points [EP $n$ s ( $n = 2, 3$ )] —EP $n$ s protected by topology that are prohibited at the non-interacting level. Specifically, we demonstrate that both bosonic and fermionic systems host such interaction-enabled EP $n$ s ( $n = 2, 3$ ) in parameter space that are protected by charge U(1), pseudo-spin-parity, and  $PT$  symmetries. The interaction-enabled EP2s are protected by zero-dimensional topology and give rise to qualitative changes in the loss rate, an experimentally measurable quantity for cold atoms. Furthermore, we reveal that interactions enable EP3s protected by one-dimensional topology beyond the point-gap topological classifications, suggesting the potential presence of a broader class of interaction-enabled non-Hermitian degeneracies.

*Introduction*.—Over the past few decades, extensive efforts have revealed that the interplay between many-body interactions and Hermitian topology gives rise to a variety of exotic phenomena that do not emerge in non-interacting systems [1–7]. Among them, it has been found that correlations can change topological classifications that provide a unified understanding of non-interacting topological insulators [8–10]. For instance, correlations can reduce the number of possible topological phases; for one-dimensional topological superconductors of symmetry class BDI, the  $\mathbb{Z}$  classification in the non-interacting case is reduced to  $\mathbb{Z}_8$  due to strong correlations [1]. Furthermore, correlations also enable topological phases that are prohibited at the non-interacting level; for one-dimensional topological superconductor of class BDI with inversion symmetry, the classification result changes from 0 to  $\mathbb{Z}_2$  due to strong correlations [11]. Correlation effects on topological classifications have been explored in higher dimensions [4–7] and further generalized to include topology in parameter space [12–14], as exemplified by the classification of topological pumps under strong correlations [15].

While many-body correlations induce rich topological phases in Hermitian systems, non-Hermiticity has opened a parallel avenue in non-interacting systems [16–31]. In non-Hermitian systems, complex-valued eigenvalues lead to unique topology known as the point-gap topology [27–29]. The point-gap topology protects characteristic degeneracies known as exceptional points (EPs) [32–37]. At these points, as well as eigenvalues, two eigenstates coalesce, resulting in the dispersion relation with a fractional exponent [38–42]. This type of unique non-Hermitian degeneracies is further extended to  $n$ -fold exceptional points (EP $n$ s with  $n \geq 3$ ) [43–47], or higher-order EPs, which are protected by topology beyond the point-gap topological classifications [43, 47]. These EPs are realized in a wide variety of systems ranging from classical metamaterials [48–58] to open quantum systems [59–72],

including NV centers [65, 66] and cold atoms [67–72]. In particular, for cold atoms, the high controllability allows access to the non-Hermitian topology under correlations in parameter space [71, 72].

The above progress naturally raises the following crucial question: *can correlated EPs emerge without non-interacting counterparts?* Although correlation effects on topology unique to non-Hermitian systems have been addressed so far [73–88], interaction-enabled topology remains largely unexplored, especially in the context of  $n$ -fold EPs with  $n \geq 3$ .

In this letter, we propose a novel type of non-Hermitian degeneracies, dubbed interaction-enabled EP $n$ s ( $n = 2, 3$ ) —EPs protected by non-Hermitian topology that are prohibited at the non-interacting level. Specifically, analyzing second-quantized Hamiltonians, we demonstrate the emergence of interaction-enabled EP $n$ s ( $n = 2, 3$ ) in parameter space for both bosonic and fermionic systems with charge U(1), pseudo-spin-parity, and  $PT$  symmetries. The interaction-enabled EP2s are protected by zero-dimensional topology and give rise to a qualitative difference in loss rate, an experimentally measurable quantity for cold atoms. Furthermore, we demonstrate that interactions enable EP3s protected by one-dimensional topology beyond the point-gap topological classifications, suggesting the potential presence of a broader class of interaction-enabled non-Hermitian degeneracies.

*Interaction-enabled zero-dimensional point-gap topology*.—We consider a two-component bosonic system in a two-dimensional parameter space  $\lambda = (x, y)$ , where  $x$  and  $y$  are real parameters. The second-quantized Hamiltonian is written as

$$\hat{H}(\lambda) = \hat{H}_0(\lambda) + \hat{H}_{\text{int}}, \quad (1)$$

where  $\hat{H}_0$  denotes the quadratic (non-interacting) part and  $\hat{H}_{\text{int}}$  represents the many-body interaction. We im-

\* [kato.musashi.52d@st.kyoto-u.ac.jp](mailto:kato.musashi.52d@st.kyoto-u.ac.jp)

† [yoshida.tsuneya.2z@kyoto-u.ac.jp](mailto:yoshida.tsuneya.2z@kyoto-u.ac.jp)

pose the following symmetries on  $\hat{H}(\lambda)$ :

$$[\hat{H}(\lambda), \hat{N}] = 0, \quad (2)$$

$$[\hat{H}(\lambda), (-1)^{\hat{T}_z}] = 0, \quad (3)$$

$$\hat{P}\hat{T}\hat{H}(\lambda)(\hat{P}\hat{T})^{-1} = \hat{H}(\lambda). \quad (4)$$

Here,  $\hat{P}\hat{T}$  is an antiunitary operator satisfying  $(\hat{P}\hat{T})^2 = \mathbb{1}$ , where  $\mathbb{1}$  denotes the identity operator. It can be represented as the product of a unitary operator and the complex conjugation operator  $\mathcal{K}$  ( $\mathcal{K}i = -i\mathcal{K}$ ). The operators  $\hat{N}$  and  $\hat{T}_z$  denote the total particle-number operator and the pseudo-spin operator, respectively, and are defined as  $\hat{N} = \hat{N}_A + \hat{N}_B$ ,  $\hat{T}_z = (\hat{N}_A - \hat{N}_B)/2$ , where  $\hat{N}_A$  ( $\hat{N}_B$ ) is the particle-number operator for the A (B) component. We further assume that these operators satisfy the following relations with the  $PT$  operator:

$$[\hat{P}\hat{T}, \hat{N}] = 0, \quad (5)$$

$$\{\hat{P}\hat{T}, \hat{T}_z\} = 0. \quad (6)$$

Here, for arbitrary operators  $\hat{A}$  and  $\hat{B}$ , the commutation and anticommutation relations are denoted by  $[\hat{A}, \hat{B}] = \hat{A}\hat{B} - \hat{B}\hat{A}$ ,  $\{\hat{A}, \hat{B}\} = \hat{A}\hat{B} + \hat{B}\hat{A}$ , respectively.

An analysis of the zero-dimensional point-gap topology reveals that correlations change the allowed topological structures:

$$0 \rightarrow \mathbb{Z}_2 \quad \text{for } N + 1 + \sigma = 0 \pmod{4}, \quad (7a)$$

$$\mathbb{Z}_2 \rightarrow \mathbb{Z}_2 \quad \text{for } N + 1 + \sigma = 2 \pmod{4}, \quad (7b)$$

$$0 \rightarrow 0 \quad \text{for } N + 1 + \sigma = 1, 3 \pmod{4}, \quad (7c)$$

where  $N$  and  $\sigma$  denote eigenvalues of  $\hat{N}$  and  $(-1)^{\hat{N}_B} = (-1)^{\hat{N}/2 - \hat{T}_z}$ , respectively. In particular, for  $N + 1 + \sigma = 0 \pmod{4}$ , interactions enable the nontrivial point-gap topology, which we see in detail below (for other cases, see Sec. S1 of Supplemental Material [89]).

Firstly, we block-diagonalize the second-quantized Hamiltonian. In correlated cases, Eqs. (2) and (3) imply that the Hamiltonian  $\hat{H} = \hat{H}_0 + \hat{H}_{\text{int}}$  commutes with both  $\hat{N}$  and  $(-1)^{\hat{N}_B}$ , indicating that  $\hat{H}$  can be block-diagonalized in Fock space into sectors labeled by their eigenvalues  $N$  and  $\sigma$ ;  $\hat{H} = \bigoplus_{N,\sigma} H_{(N,\sigma)}$ . In the non-interacting case, the Hamiltonian  $\hat{H} = \hat{H}_0$  satisfies an additional symmetry  $[\hat{H}_0, \hat{T}_z] = 0$ . This property follows from the symmetry constraint [Eq. (3)] and from the fact that  $\hat{H}_0$  is quadratic in the creation and annihilation operators. Therefore, in the absence of interactions,  $H_{(N,\sigma)}$  can be further block-diagonalized by  $\hat{T}_z$ ;  $H_{(N,\sigma)} = \bigoplus_{T_z} H_{0(N,\sigma,T_z)}$  with  $T_z$  being the eigenvalues of  $\hat{T}_z$ . Because of the anticommutation relation,  $\{\hat{P}\hat{T}, \hat{T}_z\} = 0$ , the  $PT$  symmetry is not closed within the sector with a finite value of  $T_z$ .

Let us focus on the case for  $N + 1 + \sigma = 0 \pmod{4}$ . In the absence of interactions, within this Fock-space sector

$\hat{P}\hat{T}$  and  $\hat{H}$  are represented as

$$PT_{(N,\sigma)} = \begin{pmatrix} O & p^{*-1} \\ p & O \end{pmatrix} \mathcal{K}, \quad (8)$$

$$H_{(N,\sigma)} = \begin{pmatrix} H_{0+(N,\sigma)} & O \\ O & H_{0-(N,\sigma)} \end{pmatrix}. \quad (9)$$

Here,  $O$  denotes the zero matrix,  $p$  is a unitary operator. The matrices  $H_{0+(N,\sigma)}$  and  $H_{0-(N,\sigma)}$  represent the Hamiltonian acting on the subspaces of the Fock-space sector  $(N, \sigma)$  with positive (+) and negative (-) eigenvalues of  $\hat{T}_z$ , respectively. We note that the subspace of  $T_z = 0$  is not included since  $\hat{T}_z$  is odd for  $N + 1 + \sigma = 0 \pmod{4}$ . The zero-dimensional topology of the  $H_{(N,\sigma)}$  is characterized by the topological index [27, 28, 35, 78]

$$\nu_{(N,\sigma)}(E_{\text{ref}}) := \text{sgn}(\det[H_{(N,\sigma)} - E_{\text{ref}}\mathbb{1}]), \quad (10)$$

with  $E_{\text{ref}} \in \mathbb{R}$ .

The above facts lead to a change of the zero-dimensional topological classification from 0 to  $\mathbb{Z}_2$  due to interactions, indicating the emergence of interaction-enabled EP2s [two-fold exceptional lines (EL2s)] in one-[two]-dimensional parameter space [40–42]. In non-interacting cases, the nontrivial  $\mathbb{Z}_2$  topology is forbidden [i.e.,  $\nu_{(N,\sigma)}(E_{\text{ref}}) > 0$  for  $E_{\text{ref}} \in \mathbb{R}$ ] as follows from the relation  $\det[H_{(N,\sigma)} - E_{\text{ref}}\mathbb{1}] = |\det[H_{0+(N,\sigma)} - E_{\text{ref}}\mathbb{1}]|^2$  [see Eqs. (8) and (9)]. On the other hand, in correlated cases,  $\mathbb{Z}_2$  topology can be nontrivial because  $H_{(N,\sigma)}$  is no longer block-diagonalized with respect to  $\hat{T}_z$ . Here, we note that for systematic characterization [36, 37, 43], the following index is more suited because of its independence from the choice of  $E_{\text{ref}}$

$$s_{(N,\sigma)}(\lambda) := \text{sgn}(\text{Disc}[\det[H_{(N,\sigma)}(\lambda) - E\mathbb{1}]]), \quad (11)$$

where “Disc” denotes the discriminant of a polynomial with respect to the variable  $E$ . Both of  $\mathbb{Z}_2$  indices  $\nu_{(N,\sigma)}(E_{\text{ref}})$  and  $s_{(N,\sigma)}(\lambda)$  characterize the zero-dimensional topology of EP2s. For details on the relation between Eqs. (10) and (11), see Sec. S2 of Supplemental Material [89].

*Interaction-enabled exceptional line*.—By analyzing a bosonic toy model, we demonstrate the emergence of interaction-enabled EL2s in two-dimensional parameter space. The Hamiltonian reads

$$\hat{H}(x, y) = \hat{H}_{0A}(x, y) + \hat{H}_{0B}(x, y) + \hat{H}_{\text{int}}, \quad (12)$$

$$\hat{H}_{0\tau} = \hat{\Psi}_{b,\tau}^\dagger h_\tau(x, y) \hat{\Psi}_{b,\tau}, \quad (13)$$

$$\begin{aligned} \hat{H}_{\text{int}} = V \sum_{i=1}^2 & (\hat{b}_{i,A}^\dagger \hat{b}_{i,B} \hat{b}_{3,A}^\dagger \hat{b}_{3,B} + \text{h.c.}) \\ & + U [(\hat{b}_{1,A}^\dagger \hat{b}_{2,B} + \hat{b}_{2,A}^\dagger \hat{b}_{1,B}) \hat{b}_{3,A}^\dagger \hat{b}_{3,B} + \text{h.c.}], \end{aligned} \quad (14)$$

with  $\hat{\Psi}_{b,\tau}^\dagger = (\hat{b}_{1,\tau}^\dagger, \hat{b}_{2,\tau}^\dagger, \hat{b}_{3,\tau}^\dagger)$  and  $\hat{b}_{i,\tau}^\dagger$  ( $\hat{b}_{i,\tau}$ ) creating (annihilating) a boson with component  $\tau$  (= A, B) at site  $i$  ( $= 1, 2, 3$ ). The interaction strengths are denoted by

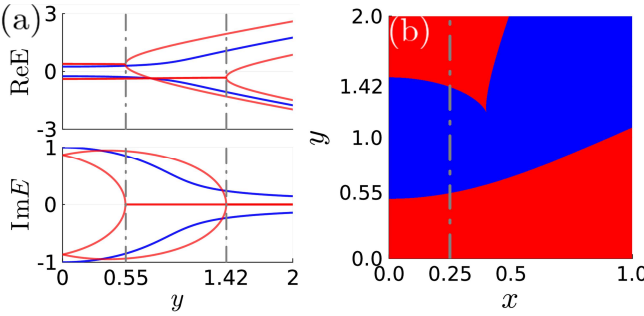


FIG. 1. (a):  $y$ -dependence of the eigenvalues of  $H_{(2,+)}(x = 0.25, y)$  for  $(w, \delta) = (0, 1)$ . The blue and red solid lines correspond to  $V = U = 0$  and  $(V, U) = (0.3, 0.5)$ , respectively. (b): The  $\mathbb{Z}_2$  topological index  $s_{(2,+)}(x, y)$  [see Eq. (11)] for  $(w, \delta) = (0, 1)$  and  $(V, U) = (0.3, 0.5)$ . The blue and red regions correspond to  $s_{(2,+)} = -1$  and  $s_{(2,+)} = +1$ , respectively.

real values  $V$  and  $U$ . The first-quantized Hamiltonian  $h_\tau(x, y)$  is given by

$$h_\tau(x, y) = \begin{pmatrix} (-1)^{\delta_{B,\tau}} x - i\delta & y & 0 \\ y & i\delta - (-1)^{\delta_{B,\tau}} x & 0 \\ 0 & 0 & w \end{pmatrix}, \quad (15)$$

with the Kronecker delta  $\delta_{\tau,\tau'}$  being equal to 1 for  $\tau = \tau'$  and 0 otherwise. The corresponding second-quantized Hamiltonian  $\hat{H}(x, y)$  preserves charge  $U(1)$ , pseudo-spin-parity, and  $PT$  symmetries [Eqs. (2)–(4)]. The  $PT$  operator is defined as

$$\hat{P}\hat{T} = \exp \left[ i \frac{\pi}{2} \sum_{i,j} \left( p_{ij} \hat{b}_{i,A}^\dagger \hat{b}_{j,B} + p_{ij}^T \hat{b}_{i,B}^\dagger \hat{b}_{j,A} \right) \right] \mathcal{K}, \quad (16)$$

with  $p = \begin{pmatrix} 0 & 1 & 0 \\ 1 & 0 & 0 \\ 0 & 0 & 1 \end{pmatrix}$ . In addition, both  $\hat{H}(x, y)$  and  $\hat{P}\hat{T}$  satisfy  $[\hat{H}(x, y), \hat{n}_3] = 0$  and  $[\hat{P}\hat{T}, \hat{n}_3] = 0$  with  $\hat{n}_3 = \sum_{\tau=A,B} \hat{b}_{3,\tau}^\dagger \hat{b}_{3,\tau}$ .

We analyze the Hamiltonian acting within the Fock-space sector with  $(N, \sigma) = (2, +)$  satisfying  $N + 1 + \sigma = 0 \pmod{4}$  and containing one particle localized on site  $i = 3$ . The basis is chosen as

$$(|A1, A3\rangle, |A2, A3\rangle, |B1, B3\rangle, |B2, B3\rangle), \quad (17)$$

with states defined as

$$|\tau i, \tau 3\rangle = \hat{b}_{i,\tau}^\dagger \hat{b}_{3,\tau}^\dagger |0\rangle. \quad (18)$$

In this Fock-space sector, the Hamiltonian is represented as

$$H_{(2,+)} = \begin{pmatrix} H_{0(2,+1)} & O \\ O & H_{0(2,+,-1)} \end{pmatrix} + H_{\text{int}(2,+)}. \quad (19)$$

Here,  $H_{0(2,+T_z)}$  ( $T_z = \pm 1$ ) is given by

$$H_{0(2,+T_z)} = w \mathbb{1}_2 + y \sigma_1 + [(-1)^{\delta_{T_z,-1}} x - i\delta] \sigma_3, \quad (20)$$

with  $\sigma_1$  and  $\sigma_3$  are the Pauli matrices. The interaction term  $H_{\text{int}(2,+)}$  is given by

$$H_{\text{int}(2,+)} = V \begin{pmatrix} 1 & & \\ & 1 & \\ 1 & & 1 \end{pmatrix} + U \begin{pmatrix} & 1 & \\ 1 & & \\ & 1 & \end{pmatrix}. \quad (21)$$

Zero matrix elements are omitted for brevity.

As an illustrative example [90], we choose  $x = 0.25$  and plot the  $y$ -dependence of the complex eigenvalues of  $H_{(2,+)}(x = 0.25, y)$  in Fig. 1(a). For  $V = U = 0$ , no degeneracy of the complex eigenvalues occurs. In contrast, for  $(V, U) = (0.3, 0.5)$ , degeneracies are observed at  $y \sim 0.55$  and  $y \sim 1.42$ , indicating the emergence of interaction-enabled EP2s. At these points, the number of complex-conjugate eigenvalue pairs changes; as  $y$  increases, the number of pairs changes from two to one at  $y \sim 0.55$  and from one to zero at  $y \sim 1.42$  [see Fig. 2(a)]. Correspondingly, the topological index  $s_{(2,+)}(x = 0.25, y)$  changes from  $+1$  to  $-1$  at  $y \sim 0.55$  and from  $-1$  to  $1$  at  $y \sim 1.42$  [see Fig. 1(b)], elucidating the topology of interaction-enabled EP2s. In addition, Fig. 1(b) indicates that these points extend to other values of  $x$ , forming the interaction-enabled EL2s.

The above results demonstrate the emergence of interaction-enabled EL2s characterized by a topological  $\mathbb{Z}_2$  index in a two-component bosonic system possessing charge  $U(1)$ , pseudo-spin-parity, and  $PT$  symmetries.

*Dynamical properties.*— The existence of interaction-enabled EL2s protected by  $PT$  symmetry is reflected in the behaviors of loss rate, an experimentally measurable quantity for cold atoms [91]. In the Fock-space sector labeled by  $(N, (-1)^{N_B}) = (2M, \sigma)$ , the loss rate of a time-independent Hamiltonian  $\hat{H}(\lambda)$  is defined as follows:

$$\langle N_{(2M,\sigma)}(t) \rangle := \text{Tr}[\hat{N} \mathcal{P}_{(2M,\sigma)} \hat{\rho}(t) \mathcal{P}_{(2M,\sigma)}], \quad (22)$$

$$L_{(2M,\sigma)}(t) := -\frac{1}{\langle N_{(2M,\sigma)}(t) \rangle} \frac{d}{dt} \langle N_{(2M,\sigma)}(t) \rangle, \quad (23)$$

where we define the density matrix as  $\hat{\rho}(t) := e^{-it\hat{H}} |\psi(0)\rangle \langle \psi(0)| e^{it\hat{H}^\dagger}$ , and  $\mathcal{P}_{(2M,\sigma)}$  is the projection operator onto the Fock-space sector with  $(2M, \sigma)$ . We also

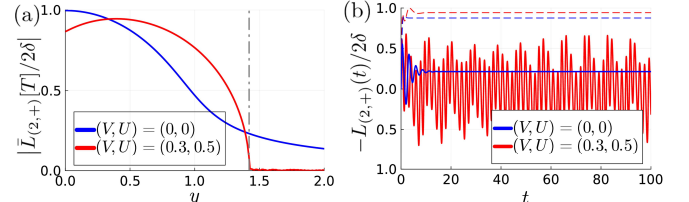


FIG. 2. (a): Dependence of  $|\bar{L}_{(2,+)}[T]/2\delta|$  on  $y$  for  $(w, \delta, x, T) = (0, 1, 0.25, 100)$ . The gray dashed line indicates  $y = 1.42$ . (b): Time dependence of  $-L_{(2,+)}(t)/2\delta$  for  $(w, \delta, x) = (0, 1, 0.25)$ . The dashed and solid lines correspond to  $y = 0.5$  and  $y = 1.5$ , respectively. In panels (a) and (b), blue and red denote the cases  $V = U = 0$  and  $(V, U) = (0.3, 0.5)$ , respectively.

introduce the time-averaged loss rate from  $t = 0$  to  $t = T$  as

$$\bar{L}_{(2M,\sigma)}[T] := \frac{1}{T} \int_0^T dt L_{(2M,\sigma)}(t). \quad (24)$$

We set the initial state as  $|\psi(0)\rangle = \frac{1}{\sqrt{2}}(|A2, A3\rangle + i|B1, B3\rangle)$  and discuss the behavior of the loss rate at  $x = 0.25$ , the same value as in Fig. 1(a).

Figure 2(a) shows that, in the interacting case,  $\bar{L}_{(2,+)}[T]$  rapidly approaches zero near  $y \sim 1.42$ , where an interaction-enabled EP2 emerges, and remains approximately zero for  $y \gtrsim 1.42$ . This behavior is due to the fact that the time-reversal loss rate satisfies  $-\bar{L}_{(2,+)}[T] \sim 2\gamma_{(2,+)}$  for sufficiently large  $T$  with  $\gamma_{(2,+)}$  being the maximum of the imaginary parts of the complex eigenvalues of  $H_{(2,+)}$  (for further details on the loss rate, see Sec. S2 of Supplemental Material [89]). These data indicate that the emergence of the interaction-enabled EL2 is reflected in the loss rate. This fact can also be found in the time-dependence of the loss rate [see Fig. 2(b)].

*Interaction-enabled EP3.*—In the above, we have discussed the emergence of interaction-enabled EL2s in two-dimensional parameter space, in which interactions play an essential role. We further extend this argument and reveal the emergence of interaction-enabled EP3s in two-dimensional parameter space, which is protected by topology beyond the point-gap topological classifications.

We consider two distinct interaction-enabled EL2s in two-dimensional parameter space, each of which corresponds to the degeneracy of a different pair of eigenvalues. Specifically, we assume that eigenvalues  $E_1$  and  $E_2$  are degenerate along one EL2, while  $E_2$  and  $E_3$  are degenerate along the other. At the point where these two EL2s intersect, three eigenvalues  $E_1$ ,  $E_2$ , and  $E_3$  become degenerate, resulting in an interaction-enabled EP3. Indeed, such a situation is observed for our toy model [see Fig. 3(a)]. We stress that in the Fock-space sector with  $(N, \sigma)$  satisfying  $N + 1 + \sigma = 0 \pmod{4}$ , EP3s are interaction-enabled, because they emerge as intersections of interaction-enabled EL2s, which is consistent with the codimension argument.

The topology of the interaction-enabled EP3 is characterized by the resultant winding number. Let us consider the characteristic polynomial  $P(E; \lambda) = \det[H(\lambda) - E\mathbb{1}_n]$  of a  $PT$ -symmetric non-Hermitian matrix  $H(\lambda) \in \mathbb{C}^{n \times n}$  ( $n \geq 3$ ). If  $H(\lambda)$  possesses an EP3 at  $\lambda = \lambda_{EP3}$ , and the corresponding eigenvalue is  $E_{EP3} \in \mathbb{R}$ , then the characteristic polynomial has a triple root at  $E = E_{EP3}$ . The topology of the triple root can be characterized by the resultant winding number

$$W_r = \oint \frac{d\lambda}{2\pi i} \cdot \partial_\lambda \ln Z_r(\lambda), \quad (25)$$

where  $Z_r$  is defined as  $Z_r(\lambda) = r_1(\lambda) + ir_2(\lambda)$  with

$$r_j(\lambda) := \text{Res} \left[ \partial_{\tilde{E}}^{2-j} P_{EP3}(\tilde{E}; \lambda), \partial_{\tilde{E}}^j P_{EP3}(\tilde{E}; \lambda) \right], \quad (26)$$

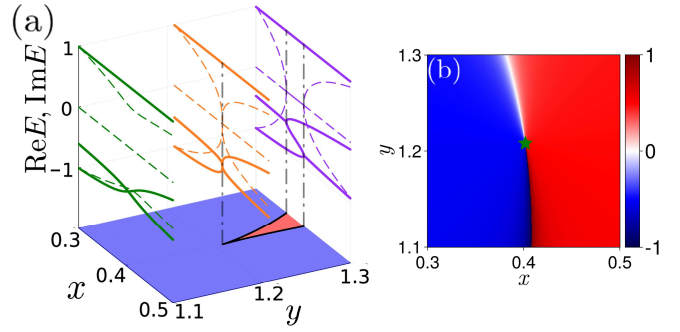


FIG. 3. (a): Real (solid) and imaginary (dashed) parts of the complex eigenvalues of  $H_{(2,+)}$  as functions of  $x$  for  $y = 1.1$ ,  $1.208$ , and  $1.3$ . For each value of  $y$ , the spectra are normalized to  $\pm 1$  over  $x \in [0.3, 0.5]$ . Blue and red regions on the bottom plane indicate  $s_{(2,+)} = -1$  and  $+1$ , respectively [see Fig. 1]; black lines denote the phase boundaries, whose intersection gives  $\lambda_{EP3} \sim (0.402, 1.208)$ . (b): Principal value of  $\arg[Z_r]/\pi$  in the  $x$ - $y$  plane. The green star marks  $\lambda_{EP3}$ . These data are obtained for  $(w, \delta, V, U) = (0, 1, 0.3, 0.5)$ .

for  $j = 1, 2$ . The integral is taken over a closed path enclosing  $\lambda = \lambda_{EP3}$ . Here,  $\text{Res}[f, g]$  denotes the resultant of two polynomials  $f$  and  $g$ . Due to  $PT$  symmetry,  $r_j$  ( $j = 1, 2$ ) are real. The polynomial of degree three  $P_{EP3}(\tilde{E}; \lambda)$  with  $\tilde{E} = E - E_{EP3}$  are obtained by the Taylor expansion of  $P(E; \lambda)$  around  $\tilde{E} = 0$ :

$$P_{EP3}(\tilde{E}; \lambda) := \sum_{k=0}^3 e'_{n-k}(\lambda) (-1)^k \tilde{E}^k \quad (27)$$

with  $e'_{k+1}$  recursively obtained from

$$(k+1)e'_{k+1}(\lambda) = \sum_{l=0}^k (-1)^l e'_{k-l}(\lambda) \text{Tr} \left[ (H'(\lambda))^{l+1} \right],$$

and  $H'(\lambda) = H(\lambda) - E_{EP3}\mathbb{1}_n$  (for more details see Sec. S3 of Supplemental Material [89]). The non-zero resultant winding number indicates that the resultants vanish  $(r_1, r_2) = \mathbf{0}$  at a point inside the closed loop where  $P_{EP3}(\tilde{E}; \lambda)$  has a triple root [43]. Computing the resultant winding number, we obtain  $W_r = -1$  [see Fig. 3(b)], elucidating the topological protection of the interaction-enabled EP3.

We finish this part with three remarks. (i) We note that our argument suggests a border class of interaction-enabled EPns. For instance, it is straightforward to generalize interaction-enabled EP4s in three-dimensional parameter space. (ii) We also note that while the resultant winding number requires the Taylor expansion around  $E_{EP3}$ , alternative winding number enables the characterization of EPns for an  $(n+1) \times (n+1)$  matrix without such an expansion for  $n \geq 3$ , thereby allowing a systematic analysis (for more details see Secs. S4 and S5 of Supplemental Material [89]). (iii) In the above, although we have restricted ourselves to bosonic systems, a similar analysis demonstrates the emergence of interaction-

enabled topology in fermionic systems (for more details, see Sec. S6 of Supplemental Material [89]).

*Summary.*—We have proposed a novel type of non-Hermitian degeneracies, dubbed interaction-enabled EP<sub>ns</sub> ( $n = 2, 3$ )—EP<sub>ns</sub> protected by topology that are prohibited at the non-interacting level. Specifically, analyzing second-quantized Hamiltonians, we have demonstrated that both bosonic and fermionic systems can host such interaction-enabled EP<sub>ns</sub> in parameter space that are protected by charge U(1), pseudo-spin-parity, and  $PT$  symmetries. Interaction-enabled EP2s are protected by zero-dimensional topology and give rise to qualitative changes in the loss rate, an experimentally measurable quantity for cold atoms. Furthermore, we have revealed that interactions enable EP3s protected

by topology beyond the point-gap topological classifications, which suggest the potential presence of a broader class of interaction-enabled EP<sub>ns</sub>.

We conclude this paper by noting that identifying feasible platforms for interaction-enabled EP<sub>ns</sub> is an important step toward their experimental observation. Among the various non-Hermitian systems, cold atoms are considered as a potential platform where an EP3 in parameter space is reported [69]. A detailed analysis along this direction is left for future work.

*Acknowledgments.*—This work is supported by JSPS KAKENHI Grant Nos. JP21K13850, JP23KK0247, JP25K07152, and JP25H02136, as well as JSPS Bilateral Program No. JPJSBP120249925. T. Y. is grateful for the support from the ETH Pauli Center for Theoretical Studies and the Grant from Yamada Science Foundation.

---

[1] L. Fidkowski and A. Kitaev, Topological phases of fermions in one dimension, *Phys. Rev. B* **83**, 075103 (2011).

[2] V. Gurarie, Single-particle Green's functions and interacting topological insulators, *Phys. Rev. B* **83**, 085426 (2011).

[3] A. M. Turner, F. Pollmann, and E. Berg, Topological phases of one-dimensional fermions: An entanglement point of view, *Phys. Rev. B* **83**, 075102 (2011).

[4] H. Yao and S. Ryu, Interaction effect on topological classification of superconductors in two dimensions, *Phys. Rev. B* **88**, 064507 (2013).

[5] Y.-Z. You and C. Xu, Symmetry-protected topological states of interacting fermions and bosons, *Phys. Rev. B* **90**, 245120 (2014).

[6] C. Wang, A. C. Potter, and T. Senthil, Classification of Interacting Electronic Topological Insulators in Three Dimensions, *Science* **343**, 629 (2014).

[7] T. Morimoto, A. Furusaki, and C. Mudry, Breakdown of the topological classification  $\mathbb{Z}$  for gapped phases of non-interacting fermions by quartic interactions, *Phys. Rev. B* **92**, 125104 (2015).

[8] A. P. Schnyder, S. Ryu, A. Furusaki, and A. W. W. Ludwig, Classification of topological insulators and superconductors in three spatial dimensions, *Phys. Rev. B* **78**, 195125 (2008).

[9] A. Kitaev, Periodic table for topological insulators and superconductors, *AIP Conf. Proc.* **1134**, 22 (2009).

[10] S. Ryu, A. P. Schnyder, A. Furusaki, and A. W. W. Ludwig, Topological insulators and superconductors: tenfold way and dimensional hierarchy, *New J. Phys.* **12**, 065010 (2010).

[11] M. F. Lapa, J. C. Y. Teo, and T. L. Hughes, Interaction-enabled topological crystalline phases, *Phys. Rev. B* **93**, 115131 (2016).

[12] Q. Niu and D. J. Thouless, Quantised adiabatic charge transport in the presence of substrate disorder and many-body interaction, *J. Phys. A: Math. Gen.* **17**, 2453 (1984).

[13] L. Wang, M. Troyer, and X. Dai, Topological Charge Pumping in a One-Dimensional Optical Lattice, *Phys. Rev. Lett.* **111**, 026802 (2013).

[14] M. Nakagawa, T. Yoshida, R. Peters, and N. Kawakami, Breakdown of topological Thouless pumping in the strongly interacting regime, *Phys. Rev. B* **98**, 115147 (2018).

[15] C.-M. Jian and C. Xu, Interacting Topological Insulators with Synthetic Dimensions, *Phys. Rev. X* **8**, 041030 (2018).

[16] V. M. Martinez Alvarez, J. E. Barrios Vargas, and L. E. F. Foa Torres, Non-Hermitian robust edge states in one dimension: Anomalous localization and eigenspace condensation at exceptional points, *Phys. Rev. B* **97**, 121401 (2018).

[17] S. Yao and Z. Wang, Edge States and Topological Invariants of Non-Hermitian Systems, *Phys. Rev. Lett.* **121**, 086803 (2018).

[18] S. Yao, F. Song, and Z. Wang, Non-Hermitian Chern Bands, *Phys. Rev. Lett.* **121**, 136802 (2018).

[19] F. K. Kunst, E. Edvardsson, J. C. Budich, and E. J. Bergholtz, Biorthogonal Bulk-Boundary Correspondence in Non-Hermitian Systems, *Phys. Rev. Lett.* **121**, 026808 (2018).

[20] K. Yokomizo and S. Murakami, Non-Bloch Band Theory of Non-Hermitian Systems, *Phys. Rev. Lett.* **123**, 066404 (2019).

[21] C. H. Lee and R. Thomale, Anatomy of skin modes and topology in non-Hermitian systems, *Phys. Rev. B* **99**, 201103 (2019).

[22] D. S. Borgnia, A. J. Kruchkov, and R.-J. Slager, Non-Hermitian Boundary Modes and Topology, *Phys. Rev. Lett.* **124**, 056802 (2020).

[23] K. Zhang, Z. Yang, and C. Fang, Correspondence between Winding Numbers and Skin Modes in Non-Hermitian Systems, *Phys. Rev. Lett.* **125**, 126402 (2020).

[24] N. Okuma, K. Kawabata, K. Shiozaki, and M. Sato, Topological Origin of Non-Hermitian Skin Effects, *Phys. Rev. Lett.* **124**, 086801 (2020).

[25] P.-Y. Chang, J.-S. You, X. Wen, and S. Ryu, Entanglement spectrum and entropy in topological non-hermitian systems and nonunitary conformal field theory, *Phys. Rev. Res.* **2**, 033069 (2020).

[26] K. Kawabata, T. Numasawa, and S. Ryu, Entanglement phase transition induced by the non-hermitian skin effect, *Phys. Rev. X* **13**, 021007 (2023).

[27] Z. Gong, Y. Ashida, K. Kawabata, K. Takasan, S. Higashikawa, and M. Ueda, Topological Phases of Non-Hermitian Systems, *Phys. Rev. X* **8**, 031079 (2018).

[28] K. Kawabata, K. Shiozaki, M. Ueda, and M. Sato, Symmetry and Topology in Non-Hermitian Physics, *Phys. Rev. X* **9**, 041015 (2019).

[29] H. Zhou and J. Y. Lee, Periodic table for topological bands with non-Hermitian symmetries, *Phys. Rev. B* **99**, 235112 (2019).

[30] Y. Ashida, Z. Gong, and M. Ueda, Non-Hermitian physics, *Adv. Phys.* **69**, 249 (2020).

[31] E. J. Bergholtz, J. C. Budich, and F. K. Kunst, Exceptional topology of non-Hermitian systems, *Rev. Mod. Phys.* **93**, 015005 (2021).

[32] T. Kato, *Perturbation Theory for Linear Operators*, Grundlehren der mathematischen Wissenschaften, Vol. 132 (Springer, 1966).

[33] H. Zhou, C. Peng, Y. Yoon, C. W. Hsu, K. A. Nelson, L. Fu, J. D. Joannopoulos, M. Soljačić, and B. Zhen, Observation of Bulk Fermi Arc and Polarization Half Charge from Paired Exceptional Points, *Science* **359**, 1009 (2018).

[34] H. Shen, B. Zhen, and L. Fu, Topological Band Theory for Non-Hermitian Hamiltonians, *Phys. Rev. Lett.* **120**, 146402 (2018).

[35] K. Kawabata, T. Bessho, and M. Sato, Classification of Exceptional Points and Non-Hermitian Topological Semimetals, *Phys. Rev. Lett.* **123**, 066405 (2019).

[36] C. C. Wojcik, X.-Q. Sun, T. Bzdušek, and S. Fan, Homotopy characterization of non-Hermitian Hamiltonians, *Phys. Rev. B* **101**, 205417 (2020).

[37] Z. Yang, A. P. Schnyder, J. Hu, and C.-K. Chiu, Fermion Doubling Theorems in Two-Dimensional Non-Hermitian Systems for Fermi Points and Exceptional Points, *Phys. Rev. Lett.* **126**, 086401 (2021).

[38] V. Kozii and L. Fu, Non-Hermitian topological theory of finite-lifetime quasiparticles: Prediction of bulk Fermi arc due to exceptional point, *Phys. Rev. B* **109**, 235139 (2024).

[39] T. Yoshida, R. Peters, and N. Kawakami, Non-Hermitian perspective of the band structure in heavy-fermion systems, *Phys. Rev. B* **98**, 035141 (2018).

[40] T. Yoshida, R. Peters, N. Kawakami, and Y. Hatsugai, Symmetry-protected exceptional rings in two-dimensional correlated systems with chiral symmetry, *Phys. Rev. B* **99**, 121101 (2019).

[41] J. C. Budich, J. Carlström, F. K. Kunst, and E. J. Bergholtz, Symmetry-protected nodal phases in non-Hermitian systems, *Phys. Rev. B* **99**, 041406 (2019).

[42] R. Okugawa and T. Yokoyama, Topological exceptional surfaces in non-Hermitian systems with parity-time and parity-particle-hole symmetries, *Phys. Rev. B* **99**, 041202 (2019).

[43] P. Delplace, T. Yoshida, and Y. Hatsugai, Symmetry-Protected Multifold Exceptional Points and Their Topological Characterization, *Phys. Rev. Lett.* **127**, 186602 (2021).

[44] I. Mandal and E. J. Bergholtz, Symmetry and Higher-Order Exceptional Points, *Phys. Rev. Lett.* **127**, 186601 (2021).

[45] S. Sayyad and F. K. Kunst, Realizing exceptional points of any order in the presence of symmetry, *Phys. Rev. Res.* **4**, 023130 (2022).

[46] A. Montag and F. K. Kunst, Symmetry-induced higher-order exceptional points in two dimensions, *Phys. Rev. Res.* **6**, 023205 (2024).

[47] T. Yoshida, J. L. K. König, L. Rødland, E. J. Bergholtz, and M. Ståhlhammar, Winding topology of multifold exceptional points, *Phys. Rev. Res.* **7**, L012021 (2025).

[48] C. Dembowski, H.-D. Gräf, H. L. Harney, A. Heine, W. D. Heiss, H. Rehfeld, and A. Richter, Experimental Observation of the Topological Structure of Exceptional Points, *Phys. Rev. Lett.* **86**, 787 (2001).

[49] S.-B. Lee, J. Yang, S. Moon, S.-Y. Lee, J.-B. Shim, S. W. Kim, J.-H. Lee, and K. An, Observation of an exceptional point in a chaotic optical microcavity, *Phys. Rev. Lett.* **103**, 134101 (2009).

[50] L. Xiao, X. Zhan, Z. H. Bian, K. K. Wang, X. Zhang, X. P. Wang, J. Li, K. Mochizuki, D. Kim, N. Kawakami, W. Yi, H. Obuse, B. C. Sanders, and P. Xue, Observation of topological edge states in parity-time-symmetric quantum walks, *Nature Physics* **13**, 1117 (2017).

[51] W. Chen, S. K. Özdemir, G. Zhao, J. Wiersig, and L. Yang, Exceptional points enhance sensing in an optical microcavity, *Nature* **548**, 192 (2017).

[52] H. Hodaei, A. U. Hassan, S. Wittek, H. Garcia-Gracia, R. El-Ganainy, D. N. Christodoulides, and M. Khajavikhan, Enhanced sensitivity at higher-order exceptional points, *Nature* **548**, 187 (2017).

[53] M.-A. Miri and A. Alù, Exceptional points in optics and photonics, *Science* **363**, eaar7709 (2019).

[54] J. Doppler, A. A. Mailybaev, J. Böhm, U. Kuhl, A. Girschik, F. Libisch, T. J. Milburn, P. Rabl, N. Moiseyev, and S. Rotter, Dynamically encircling an exceptional point for asymmetric mode switching, *Nature* **537**, 76 (2016).

[55] X.-L. Zhang, T. Jiang, and C. T. Chan, Dynamically encircling an exceptional point in anti-parity-time symmetric systems: asymmetric mode switching for symmetry-broken modes, *Light: Sci. Appl.* **8**, 88 (2019).

[56] K. Ding, G. Ma, M. Xiao, Z. Q. Zhang, and C. T. Chan, Emergence, Coalescence, and Topological Properties of Multiple Exceptional Points and Their Experimental Realization, *Phys. Rev. X* **6**, 021007 (2016).

[57] W. Tang, X. Jiang, K. Ding, Y.-X. Xiao, Z.-Q. Zhang, C. T. Chan, and G. Ma, Exceptional nexus with a hybrid topological invariant, *Science* **370**, 1077 (2020).

[58] W. Tang, K. Ding, and G. Ma, Realization and topological properties of third-order exceptional lines embedded in exceptional surfaces, *Nat. Commun.* **14**, 6660 (2023).

[59] M. Naghiloo, M. Abbasi, Y. N. Joglekar, and K. W. Murch, Quantum state tomography across the exceptional point in a single dissipative qubit, *Nat. Phys.* **15**, 1232 (2019).

[60] W. Chen, M. Abbasi, B. Ha, S. Erdamar, Y. N. Joglekar, and K. W. Murch, Decoherence-Induced Exceptional Points in a Dissipative Superconducting Qubit, *Phys. Rev. Lett.* **128**, 110402 (2022).

[61] P.-R. Han, W. Ning, X.-J. Huang, R.-H. Zheng, S.-B. Yang, F. Wu, Z.-B. Yang, Q.-P. Su, C.-P. Yang, and S.-B. Zheng, Measuring topological invariants for higher-order exceptional points in quantum three-mode systems, *Nat. Commun.* **15**, 10293 (2024).

[62] L. Ding, K. Shi, Q. Zhang, D. Shen, X. Zhang, and W. Zhang, Experimental Determination of  $\mathcal{PT}$ -Symmetric Exceptional Points in a Single Trapped Ion, *Phys. Rev. Lett.* **126**, 083604 (2021).

[63] P. Lu, Y. Liu, Q. Lao, T. Liu, X. Rao, J. Bian, H. Wu, F. Zhu, and L. Luo, Dynamical topology of chiral and nonreciprocal state transfers in a non-Hermitian quantum system, *Commun. Phys.* **8**, 91 (2025).

[64] Y.-Y. Chen, K. Li, L. Zhang, Y.-K. Wu, J.-Y. Ma, H.-X. Yang, C. Zhang, B.-X. Qi, Z.-C. Zhou, P.-Y. Hou, Y. Xu, and L.-M. Duan, Quantum tomography of a third-order exceptional point in a dissipative trapped ion, *Nat. Commun.* **16**, 7478 (2025).

[65] W. Liu, Y. Wu, C.-K. Duan, X. Rong, and J. Du, Dynamically Encircling an Exceptional Point in a Real Quantum System, *Phys. Rev. Lett.* **126**, 170506 (2021).

[66] Y. Wu, Y. Wang, X. Ye, W. Liu, Z. Niu, C.-K. Duan, Y. Wang, X. Rong, and J. Du, Third-order exceptional line in a nitrogen-vacancy spin system, *Nat. Nanotechnol.* **19**, 160 (2024).

[67] J. Li, A. K. Harter, J. Liu, L. de Melo, Y. N. Joglekar, and L. Luo, Observation of parity-time symmetry breaking transitions in a dissipative Floquet system of ultracold atoms, *Nat. Commun.* **10**, 855 (2019).

[68] Z. Ren, D. Liu, E. Zhao, C. He, K. K. Pak, J. Li, and G.-B. Jo, Chiral control of quantum states in non-Hermitian spin-orbit-coupled fermions, *Nat. Phys.* **18**, 385 (2022).

[69] C. Wang, N. Li, J. Xie, C. Ding, Z. Ji, L. Xiao, S. Jia, B. Yan, Y. Hu, and Y. Zhao, Exceptional Nexus in Bose-Einstein Condensates with Collective Dissipation, *Phys. Rev. Lett.* **132**, 253401 (2024).

[70] E. Zhao, Z. Wang, C. He, T. F. J. Poon, K. K. Pak, Y.-J. Liu, P. Ren, X.-J. Liu, and G.-B. Jo, Two-dimensional non-Hermitian skin effect in an ultracold Fermi gas, *Nature* **637**, 565 (2025).

[71] J. Zhang, E.-Z. Li, Y.-J. Wang, B. Liu, L.-H. Zhang, Z.-Y. Zhang, S.-Y. Shao, Q. Li, H.-C. Chen, Y. Ma, T.-Y. Han, Q.-F. Wang, J.-D. Nan, Y.-M. Yin, D.-Y. Zhu, G.-C. Guo, D.-S. Ding, and B.-S. Shi, Exceptional Point and Hysteresis Trajectories in Cold Rydberg Atomic Gases, *Nat. Commun.* **16**, 3511 (2025).

[72] T. Chen, C. Huang, J. P. Covey, and B. Gadway, Collective Dissipation Engineering of Interacting Rydberg Atoms, *Phys. Rev. Lett.* **135**, 253402 (2025).

[73] P. A. McClarty and J. G. Rau, Non-Hermitian topology of spontaneous magnon decay, *Phys. Rev. B* **100**, 100405 (2019).

[74] S. Mu, C. H. Lee, L. Li, and J. Gong, Emergent Fermi surface in a many-body non-Hermitian fermionic chain, *Phys. Rev. B* **102**, 081115 (2020).

[75] W. N. Faugno and T. Ozawa, Interaction-Induced Non-Hermitian Topological Phases from a Dynamical Gauge Field, *Phys. Rev. Lett.* **129**, 180401 (2022).

[76] R. Shen and C. H. Lee, Non-Hermitian skin clusters from strong interactions, *Commun. Phys.* **5**, 238 (2022).

[77] S.-B. Zhang, M. M. Denner, T. c. v. Bzdušek, M. A. Sentef, and T. Neupert, Symmetry breaking and spectral structure of the interacting Hatano-Nelson model, *Phys. Rev. B* **106**, L121102 (2022).

[78] K. Kawabata, K. Shiozaki, and S. Ryu, Many-body topology of non-Hermitian systems, *Phys. Rev. B* **105**, 165137 (2022).

[79] S. Hamanaka, K. Yamamoto, and T. Yoshida, Interaction-induced Liouvillian skin effect in a fermionic chain with a two-body loss, *Phys. Rev. B* **108**, 155114 (2023).

[80] T. Yoshida and Y. Hatsugai, Fate of exceptional points under interactions: Reduction of topological classifications, *Phys. Rev. B* **107**, 075118 (2023).

[81] T. Yoshida, S.-B. Zhang, T. Neupert, and N. Kawakami, Non-Hermitian Mott Skin Effect, *Phys. Rev. Lett.* **133**, 076502 (2024).

[82] B. H. Kim, J.-H. Han, and M. J. Park, Collective non-Hermitian skin effect: point-gap topology and the doublon-holon excitations in non-reciprocal many-body systems, *Commun. Phys.* **7**, 73 (2024).

[83] C. Ekman and E. J. Bergholtz, Liouvillian skin effects and fragmented condensates in an integrable dissipative Bose-Hubbard model, *Phys. Rev. Res.* **6**, L032067 (2024).

[84] A. M. García-García, L. Sá, J. J. M. Verbaarschot, and C. Yin, Emergent topology in many-body dissipative quantum matter, *Phys. Rev. B* **111**, 035157 (2025).

[85] W.-Z. Ling, Z.-F. Cai, and T. Liu, Interaction-induced second-order skin effect, *Phys. Rev. B* **111**, 205418 (2025).

[86] L. Pan, S. Chen, and X. Cui, Interacting non-Hermitian ultracold atoms in a harmonic trap: Two-body exact solution and a high-order exceptional point, *Phys. Rev. A* **99**, 063616 (2019).

[87] D. J. Luitz and F. Piazza, Exceptional points and the topology of quantum many-body spectra, *Phys. Rev. Res.* **1**, 033051 (2019).

[88] R. Schäfer, J. C. Budich, and D. J. Luitz, Symmetry protected exceptional points of interacting fermions, *Phys. Rev. Res.* **4**, 033181 (2022).

[89] Supplemental Material presents details of numerical simulations, dynamical properties, and topological invariants.

[90] Since the spectrum is symmetric about  $x$  and  $y$  axes, we focus on the first quadrant.

[91] Y. Takasu, T. Yagami, Y. Ashida, R. Hamazaki, Y. Kuno, and Y. Takahashi, PT-symmetric non-Hermitian quantum many-body system using ultracold atoms in an optical lattice with controlled dissipation, *Prog. Theor. Exp. Phys.* **2020**, 12A110 (2020).

Supplemental Material:  
**Interaction-Enabled Two- and Three-Fold Exceptional Points**

**S1. SYMMETRIES AND TOPOLOGY ON THE FOCK-SPACE SECTOR WITH  $(N, \sigma)$**

Here, we consider both bosonic and fermionic non-Hermitian systems possessing charge  $U(1)$ , pseudo-spin-parity, and  $PT$  symmetries. Accordingly, the second-quantized Hamiltonian  $\hat{H} = \hat{H}_0 + \hat{H}_{\text{int}}$  satisfies the following relations:

$$[\hat{H}, \hat{N}] = 0, \quad (\text{S1})$$

$$[\hat{H}, (-1)^{\hat{T}_z}] = 0, \quad (\text{S2})$$

$$[\hat{P}\hat{T}, \hat{H}] = 0. \quad (\text{S3})$$

Here, we assume that the  $PT$  operator satisfies

$$(\hat{P}\hat{T})^2 = 1, \quad (\text{S4})$$

$$[\hat{P}\hat{T}, \hat{N}] = 0, \quad (\text{S5})$$

$$\{\hat{P}\hat{T}, \hat{T}_z\} = 0. \quad (\text{S6})$$

The total particle-number operator  $\hat{N}$  and the pseudo-spin operator  $\hat{T}_z$  are defined as

$$\hat{N} := \hat{N}_A + \hat{N}_B, \quad (\text{S7})$$

$$\hat{T}_z := \frac{1}{2}(\hat{N}_A - \hat{N}_B), \quad (\text{S8})$$

$$\hat{N}_\tau := \sum_i \hat{a}_{i,\tau}^\dagger \hat{a}_{i,\tau}. \quad (\text{S9})$$

The operators  $\hat{a}_{i,\tau}^\dagger$  and  $\hat{a}_{i,\tau}$  denote the creation and annihilation operators of particles in component  $\tau$  ( $= A, B$ ), respectively. These operators obey bosonic commutation relations or fermionic anticommutation relations, depending on the statistics of the particles.

Under the above symmetry conditions,  $\hat{H}$  commutes with  $\hat{N}$  and  $(-1)^{\hat{N}_B}$  ( $\hat{N}_B = \hat{N}/2 - \hat{T}_z$ ), and can hence be block-diagonalized as

$$\hat{H} = \bigoplus_{N=0,1,\dots} \bigoplus_{\sigma=\pm} H_{(N,\sigma)}, \quad (\text{S10})$$

where  $N$  and  $\sigma$  denote the eigenvalues of  $\hat{N}$  and  $(-1)^{\hat{N}_B}$ , respectively. Furthermore, in the absence of interactions,  $\hat{H} = \hat{H}_0$  can be expressed as a quadratic form of the creation and annihilation operators. From the commutation of  $\hat{H}$  with  $(-1)^{\hat{T}_z}$ , it follows that the corresponding first-quantized free-particle Hamiltonian  $h$  commutes with the first-quantized pseudo-spin operator  $t_z$ , i.e.,  $[h, t_z] = 0$ . This implies  $[\hat{H}, \hat{T}_z] = 0$ , which in turn allows  $H_{(N,\sigma)}$  to be further block-diagonalized as

$$H_{(N,\sigma)} = \bigoplus_{T_z} H_{0(N,\sigma,T_z)}, \quad (\text{S11})$$

where  $T_z$  denotes the eigenvalues of  $\hat{T}_z$ .

Considering the zero-dimensional point-gap topology of the Hamiltonian  $H_{(N,\sigma)}$ , we find

$$0 \rightarrow \mathbb{Z}_2 \quad \text{for } N+1+\sigma = 0 \pmod{4}, \quad (\text{S12})$$

$$\mathbb{Z}_2 \rightarrow \mathbb{Z}_2 \quad \text{for } N+1+\sigma = 2 \pmod{4}, \quad (\text{S13})$$

$$0 \rightarrow 0 \quad \text{for } N+1+\sigma = 1, 3 \pmod{4}, \quad (\text{S14})$$

where the topology on the left (right) side of each arrow corresponds to the non-interacting (interacting) case. In the following, we explain the details of this result.

### A. $PT$ symmetry and the Fock-space sector labeled by $(N, \sigma)$

Firstly, we analyze the action of  $\hat{P}\hat{T}$  on the subspace labeled by  $(N, \sigma)$ . From Eqs. (S5) and (S6), we obtain

$$\hat{P}\hat{T}(-1)^{\hat{N}_B}(\hat{P}\hat{T})^{-1} = (-1)^{\hat{N}}(-1)^{\hat{N}_B}. \quad (\text{S15})$$

It then follows that the action of  $\hat{P}\hat{T}$  is closed within the  $(N, \sigma)$ -labeled Fock-space sector when  $N$  is even, while it is not closed when  $N$  is odd.

Let us consider the case where  $N$  is even. In this case, the action of  $\hat{P}\hat{T}$  is closed within the Fock-space sector labeled by  $(N, \sigma)$ . However, for the Fock-space sector labeled by  $(N, \sigma, T_z)$ , the anticommutation relation  $\{\hat{P}\hat{T}, \hat{T}_z\} = 0$  implies that the action of  $\hat{P}\hat{T}$  maps the  $(N, \sigma, T_z)$  subspace to the  $(N, \sigma, -T_z)$  subspace. In other words, only the Fock-space sector with finite  $T_z = 0$  is closed under the  $PT$  operation. Moreover, due to  $PT$  symmetry, the bases of the  $(N, \sigma, T_z)$  and  $(N, \sigma, -T_z)$  subspaces are in one-to-one correspondence, and thus the dimensions of these subspaces are equal. Next, we examine under which conditions the  $(N, \sigma)$ -labeled Fock-space sector contains a  $T_z = 0$  subspace. By introducing a non-negative integer  $M$  such that  $N = 2M$ ,  $T_z$  can be expressed as  $T_z = M - N_B$ , where  $N_B$  denotes the eigenvalues of  $\hat{N}_B$ . In a subspace with fixed  $(-1)^{N_B} = \sigma$ ,  $N_B$  can take either only even or only odd values. From this analysis, the  $(N, \sigma)$ -labeled Fock-space sector does not contain a  $T_z = 0$  subspace in the following cases: (i)  $M$  is even and  $\sigma = -$ , or (ii)  $M$  is odd and  $\sigma = +$ . These cases can be collectively expressed as  $N + 1 + \sigma = 0 \pmod{4}$ . On the other hand, the  $(N, \sigma)$ -labeled Fock-space sector contains a  $T_z = 0$  subspace in the following cases: (i)  $M$  is even and  $\sigma = +$ , or (ii)  $M$  is odd and  $\sigma = -$ , which can be collectively expressed as  $N + 1 + \sigma = 2 \pmod{4}$ .

For odd  $N$ , as stated at the beginning of this section, the action of  $\hat{P}\hat{T}$  is not closed within the  $(N, \sigma)$  Fock-space sector. In this case, we have  $N + 1 + \sigma = 1, 3 \pmod{4}$ .

We next provide an explicit example of a many-body  $\hat{P}\hat{T}$  operator satisfying  $(\hat{P}\hat{T})^2 = \mathbb{1}$ ,  $[\hat{P}\hat{T}, \hat{N}] = 0$  and  $\{\hat{P}\hat{T}, \hat{T}_z\} = 0$ . Let  $p$  be a real orthogonal matrix ( $p^T p = \mathbb{1}$ ), and consider

$$\hat{P}\hat{T} = e^{i\frac{\pi}{2}\hat{Q}}\mathcal{K}, \quad (\text{S16})$$

$$\hat{Q} = \sum_{i,j} (p_{ij}\hat{a}_{i,A}^\dagger\hat{a}_{j,B} + p_{ij}^T\hat{a}_{i,B}^\dagger\hat{a}_{j,A}), \quad (\text{S17})$$

where  $\mathcal{K}$  denotes the complex conjugation operator, and  $\hat{a}_{j,\tau}^\dagger$  ( $\hat{a}_{j,\tau}$ ) denotes the creation (annihilation) operator for a boson or fermion in component  $\tau$  at site  $j$ . Since  $\hat{Q}$  is real,  $\hat{Q} = \hat{Q}^*$ , it follows that

$$(\hat{P}\hat{T})^2 = e^{i\frac{\pi}{2}\hat{Q}}e^{-i\frac{\pi}{2}\hat{Q}}\mathcal{K}^2 = \mathbb{1}. \quad (\text{S18})$$

Furthermore, one finds

$$\begin{aligned} \hat{P}\hat{T}\hat{a}_{i,A}^\dagger(\hat{P}\hat{T})^{-1} &= e^{i\frac{\pi}{2}\hat{Q}}\mathcal{K}\hat{a}_{i,A}^\dagger\mathcal{K}e^{-i\frac{\pi}{2}\hat{Q}} \\ &= \hat{a}_{i,A}^\dagger + \frac{i\pi}{2}[\hat{Q}, \hat{a}_{i,A}^\dagger] + \frac{(\frac{i\pi}{2})^2}{2!}[\hat{Q}, [\hat{Q}, \hat{a}_{i,A}^\dagger]] + \dots \\ &= \cos\left(\frac{\pi}{2}\right)\hat{a}_{i,A}^\dagger + i\sin\left(\frac{\pi}{2}\right)\sum_j \hat{a}_{j,B}^\dagger p_{ji}^T \\ &= i\sum_j \hat{a}_{j,B}^\dagger p_{ji}^T. \end{aligned} \quad (\text{S19})$$

Similarly, one obtains

$$\hat{P}\hat{T} \begin{pmatrix} \hat{a}_{i,A}^\dagger \\ \hat{a}_{i,B}^\dagger \end{pmatrix} (\hat{P}\hat{T})^{-1} = i\sum_j \begin{pmatrix} \hat{a}_{j,B}^\dagger p_{ji}^T \\ \hat{a}_{j,A}^\dagger p_{ji} \end{pmatrix}, \quad (\text{S20})$$

$$\hat{P}\hat{T} \begin{pmatrix} \hat{a}_{i,A} \\ \hat{a}_{i,B} \end{pmatrix} (\hat{P}\hat{T})^{-1} = -i\sum_j \begin{pmatrix} p_{ij}\hat{a}_{j,B} \\ p_{ij}^T\hat{a}_{j,A} \end{pmatrix}. \quad (\text{S21})$$

From these expressions, it is straightforward to verify that the  $\hat{P}\hat{T}$  operator defined in Eq. (S16) satisfies  $[\hat{P}\hat{T}, \hat{N}] = 0$  and  $\{\hat{P}\hat{T}, \hat{T}_z\} = 0$ .

## B. Zero-dimensional point-gap topology of $H_{(N,\sigma)}$

We now discuss the zero-dimensional point-gap topology of  $H_{(N,\sigma)}$ , which acts invariantly within each Fock-space sector labeled by  $(N, \sigma)$ . The associated topological index is defined as

$$\nu_{(N,\sigma)} = \text{sgn}(\det[H_{(N,\sigma)} - E_{\text{ref}} \mathbb{1}]), \quad (\text{S22})$$

where  $E_{\text{ref}}$  is a real reference energy.

In the absence of many-body interactions, the Hamiltonian  $\hat{H} = \hat{H}_0$ , in addition to satisfying the symmetry conditions Eqs. (S1)-(S3), also obeys

$$[\hat{H}_0, \hat{T}_z] = 0. \quad (\text{S23})$$

As a consequence,  $H_{(N,\sigma)}$  can be further block-diagonalized as in Eq. (S11). As we shall see below, this additional symmetry satisfied by  $\hat{H}_0$  leads to a qualitative difference in the point-gap topology between the noninteracting and interacting cases. As discussed in Sec. S1 A, the constraints imposed by  $\hat{P}\hat{T}$  on the Hamiltonian within each Fock-space sector labeled by  $(N, \sigma)$  depend on the value of  $N+1+\sigma \pmod{4}$ . We therefore analyze the point-gap topology separately for each case.

For the case  $N+1+\sigma = 0 \pmod{4}$ , the action of  $\hat{P}\hat{T}$  is closed within the Fock-space sector labeled by  $(N, \sigma)$ . In the absence of interactions, the Hamiltonian can be further block-diagonalized by  $\hat{T}_z$ , but there exists no subspace corresponding to the eigenvalue  $T_z = 0$ . For an arbitrary  $T_z \neq 0$ , the anticommutation relation  $\{\hat{P}\hat{T}, \hat{T}_z\} = 0$  implies that  $H_{0(N,\sigma,T_z)}$  and  $H_{0(N,\sigma,-T_z)}$  in Eq. (S11) are related by a unitary matrix  $U_{PT}$  as

$$U_{PT} H_{0(N,\sigma,T_z)}^* U_{PT}^\dagger = H_{0(N,\sigma,-T_z)}. \quad (\text{S24})$$

Therefore, the topological index  $\nu_{(N,\sigma)}$  characterizing the point-gap topology protected by  $PT$  symmetry is given by

$$\begin{aligned} \nu_{(N,\sigma)} &= \prod_{T_z} \text{sgn}(\det[H_{0(N,\sigma,T_z)} - E_{\text{ref}} \mathbb{1}]) \\ &= \prod_{T_z > 0} \text{sgn}(|\det[H_{0(N,\sigma,T_z)} - E_{\text{ref}} \mathbb{1}]|^2) = 1 \end{aligned} \quad (\text{S25})$$

and hence it cannot take the value  $-1$ . This indicates that the system is topologically trivial in the absence of interactions. On the other hand, once interactions are introduced, the block diagonalization of  $\hat{H} = \hat{H}_0 + \hat{H}_{\text{int}}$  with respect to  $\hat{T}_z$  is no longer applicable. As a result,  $\nu_{(N,\sigma)}$  can take both values  $\pm 1$ . From the above discussion, we conclude that the classification of the zero-dimensional point-gap topology of  $H_{(N,\sigma)}$  changes due to interactions as

$$0 \rightarrow \mathbb{Z}_2 \quad \text{for } N+1+\sigma = 0 \pmod{4}.$$

For the case  $N+1+\sigma = 2 \pmod{4}$ , the action of  $\hat{P}\hat{T}$  is also closed within the Fock-space sector labeled by  $(N, \sigma)$ . In the absence of interactions,  $H_{(N,\sigma)}$  can be further block-diagonalized by  $\hat{T}_z$ , and this Fock-space sector contains a subspace labeled by  $T_z = 0$ , within which the  $PT$  symmetry is closed. Accordingly,  $\nu_{(N,\sigma)}$  is given by

$$\begin{aligned} \nu_{(N,\sigma)} &= \prod_{T_z} \text{sgn}(\det[H_{0(N,\sigma,T_z)} - E_{\text{ref}} \mathbb{1}]) \\ &= \text{sgn}(\det[H_{0(N,\sigma,0)} - E_{\text{ref}} \mathbb{1}]) \times \prod_{T_z > 0} \text{sgn}(|\det[H_{0(N,\sigma,T_z)} - E_{\text{ref}} \mathbb{1}]|^2) \end{aligned} \quad (\text{S26})$$

and is therefore allowed to take both  $+1$  and  $-1$ . When interactions are introduced, the block diagonalization of  $\hat{H}$  with respect to  $\hat{T}_z$  is no longer applicable; however, the above  $\mathbb{Z}_2$  topological index remains well defined even in the presence of interactions. This suggests that the topology of  $H_{(N,\sigma)}$  is preserved under interactions. From the above discussion, the classification of the zero-dimensional point-gap topology of  $H_{(N,\sigma)}$  is given by

$$\mathbb{Z}_2 \rightarrow \mathbb{Z}_2 \quad \text{for } N+1+\sigma = 2 \pmod{4}.$$

For the cases  $N+1+\sigma = 1, 3 \pmod{4}$ , the  $PT$  symmetry is not closed within the Fock-space sector labeled by  $(N, \sigma)$  [see Eq. (S15)]. Therefore, the  $PT$ -protected  $\mathbb{Z}_2$  index is not well defined in this sector, and the zero-dimensional point-gap topology is trivial both with and without interactions. The resulting classification is

$$0 \rightarrow 0 \quad \text{for } N+1+\sigma = 1, 3 \pmod{4}.$$

## S2. PROPERTIES OF $PT$ -SYMMETRIC NON-HERMITIAN HAMILTONIANS

### A. Characteristic-polynomial discriminants and EP2s in $PT$ -symmetric systems

The discriminant of the characteristic polynomial of a matrix  $H \in \mathbb{C}^{n \times n}$  is defined by

$$\text{Disc}[\det[H - E\mathbb{1}_n]] := \prod_{1 \leq i < j \leq n} (\lambda_i - \lambda_j)^2, \quad (\text{S27})$$

with  $\{\lambda_i\}_{i=1}^n$  being the eigenvalues of  $H$ . For a  $PT$ -symmetric Hamiltonian  $H$ , its spectrum consists of real eigenvalues as well as pairs of complex-conjugate eigenvalues with positive and negative imaginary parts. Accordingly, we partition the index set labeling the eigenvalues into three disjoint subsets:  $I_1$  labeling the  $n_r$  real eigenvalues;  $I_2$  labeling the  $n_c$  eigenvalues with positive imaginary parts; and  $I_3$  labeling their complex-conjugate counterparts. With this partition, one obtains

$$\text{Disc}[\det[H - E\mathbb{1}_n]] = \prod_{\alpha=1}^3 \left( \prod_{i < j (i, j \in I_\alpha)} (\lambda_i - \lambda_j)^2 \right) \times \prod_{1 \leq \beta < \gamma \leq 3} \left( \prod_{l \in I_\beta} \prod_{k \in I_\gamma} (\lambda_l - \lambda_k)^2 \right). \quad (\text{S28})$$

In the first part on the right-hand side of the above equation, the contributions with  $\alpha = 2$  and  $\alpha = 3$  form a complex-conjugate pair. Hence, the first part is non-negative. In the second part, the contributions with  $(\beta, \gamma) = (1, 2)$  and  $(\beta, \gamma) = (1, 3)$  form a complex-conjugate pair, whereas the contribution with  $(\beta, \gamma) = (2, 3)$  can take negative values. Indeed, for  $(\beta, \gamma) = (2, 3)$ , we obtain

$$\begin{aligned} \prod_{l \in I_2} \prod_{k \in I_3} (\lambda_l - \lambda_k)^2 &= \prod_{j \in I_2} (\lambda_j - \lambda_j^*)^2 \times \prod_{l < k (l, k \in I_2)} (\lambda_l - \lambda_k^*)^2 (\lambda_k - \lambda_l^*)^2 \\ &= (-1)^{n_c} \times \prod_{j \in I_2} (2\text{Im}\lambda_j)^2 \times \prod_{l < k (l, k \in I_2)} |\lambda_l - \lambda_k^*|^4. \end{aligned} \quad (\text{S29})$$

Here, in going from the first line to the second line on the right-hand side of the above equation, we have used the fact that each eigenvalue  $\lambda_k$  with  $k \in I_3$  is in one-to-one correspondence with the complex conjugate of an eigenvalue  $\lambda_k$  with  $k \in I_2$  satisfying  $\text{Im}\lambda_k > 0$ . Therefore, the sign of the discriminant of the characteristic polynomial of a  $PT$ -symmetric  $H$  is determined by the parity of the total number  $n_c$  of complex-conjugate eigenvalue pairs.

On the other hand, for  $E_{\text{ref}} \in \mathbb{R}$ ,

$$\det[H - E_{\text{ref}}\mathbb{1}_n] = \prod_{i \in I_1} (\lambda_i - E_{\text{ref}}) \times \left| \prod_{j \in I_2} (\lambda_j - E_{\text{ref}}) \right|^2. \quad (\text{S30})$$

Thus,  $\nu = \text{sgn}(\det[H(\lambda) - E_{\text{ref}}\mathbb{1}_n])$  counts the parity of the number of real eigenvalues  $\lambda_i$  satisfying  $\lambda_i < E_{\text{ref}}$ . If  $E_{\text{ref}}$  is chosen as the EP2 eigenvalue  $E_{\text{EP2}}$  at a parameter point  $\lambda = \lambda_{\text{EP2}}$ ,  $\nu$  changes discontinuously upon crossing  $\lambda_{\text{EP2}}$ . Correspondingly, the number of complex-conjugate eigenvalue pairs changes by one, and hence  $s = \text{sgn}(\text{Disc}[\det[H(\lambda) - E\mathbb{1}_n]])$  also exhibits a discontinuous change.

### B. Behavior of the loss rate

For a non-Hermitian matrix  $H$ , we define  $B := (H - H^\dagger)/2i$  ( $= B^\dagger$ ). Then one finds

$$\text{Im}\langle \tilde{\psi}(t) | H | \tilde{\psi}(t) \rangle = \langle \tilde{\psi}(t) | B | \tilde{\psi}(t) \rangle, \quad (\text{S31})$$

where  $|\tilde{\psi}(t)\rangle = \frac{e^{-itH}|\psi(0)\rangle}{\|e^{-itH}|\psi(0)\rangle\|}$ . From this, we obtain the bound

$$\left| \text{Im}\langle \tilde{\psi}(t) | H | \tilde{\psi}(t) \rangle \right| = \left| \langle \tilde{\psi}(t) | B | \tilde{\psi}(t) \rangle \right| \leq \|B\|, \quad (\text{S32})$$

where the operator norm is defined as  $\|B\| := \max_{\||x\rangle\|=1} \|B|x\rangle\|$ . Therefore, for  $H_{(2M,\sigma)}$ , the instantaneous loss rate satisfies

$$\begin{aligned} |L_{(2M,\sigma)}(t)| &= \left| \frac{1}{\langle N_{(2M,\sigma)}(t) \rangle} \frac{d}{dt} \langle N_{(2M,\sigma)}(t) \rangle \right| \\ &= 2 \left| \text{Im} \frac{\text{Tr}[H_{(2M,\sigma)} \mathcal{P}_{(2M,\sigma)} \hat{\rho}(t) \mathcal{P}_{(2M,\sigma)}]}{\text{Tr}[\mathcal{P}_{(2M,\sigma)} \hat{\rho}(t) \mathcal{P}_{(2M,\sigma)}]} \right| \\ &= 2 \left| \text{Im} \langle \tilde{\psi}_{(2M,\sigma)}(t) | H_{(2M,\sigma)} | \tilde{\psi}_{(2M,\sigma)}(t) \rangle \right| \\ &\leq 2 \|B_{(2M,\sigma)}\|, \end{aligned} \quad (\text{S33})$$

where  $B_{(2M,\sigma)} = (H_{(2M,\sigma)} - H_{(2M,\sigma)}^\dagger)/2i$ . Similarly, the time-averaged loss rate is bounded as

$$|\bar{L}_{(2M,\sigma)}[T]| = \left| \frac{1}{T} \int_0^T dt L_{(2M,\sigma)}(t) \right| \leq 2 \|B_{(2M,\sigma)}\|. \quad (\text{S34})$$

Here,  $|\tilde{\psi}_{(2M,\sigma)}(t)\rangle = \frac{e^{-itH_{(2M,\sigma)}} \mathcal{P}_{(2M,\sigma)} |\psi\rangle}{\|e^{-itH_{(2M,\sigma)}} \mathcal{P}_{(2M,\sigma)} |\psi\rangle\|}$ . For the bosonic toy model in Eq. (S63) and the fermionic toy model in Eq. (S70), we find  $\|B_{(2,+)}\| = |\delta|$ .

We assume that the non-Hermitian Hamiltonian  $H$  is diagonalizable in terms of its right eigenvectors  $|R_n\rangle$  and left eigenvectors  $|L_n\rangle$ , such that  $H = \sum_n E_n |R_n\rangle \langle L_n|$ . Then, the time-evolved state is given by  $|\psi(t)\rangle = \sum_n l_n e^{-itE_n} |R_n\rangle$ , where  $l_n := \langle L_n | \psi(0) \rangle$ . Using this expression, we obtain

$$\begin{aligned} \text{Im} \langle \psi(t) | H | \psi(t) \rangle &= \frac{1}{2} \frac{d}{dt} \sum_{mn} l_m^* l_n \langle R_m | R_n \rangle e^{-it(E_n - E_m^*)} \\ &= \frac{1}{2} \frac{d}{dt} \sum_{mn} e^{t\beta_{mn}} Z_{mn} e^{it\alpha_{mn}}. \end{aligned} \quad (\text{S35})$$

Here, we have defined

$$\alpha_{mn} := \text{Re}E_m - \text{Re}E_n = -\alpha_{nm}, \quad (\text{S36})$$

$$\beta_{mn} := \text{Im}E_m + \text{Im}E_n = \beta_{nm}, \quad (\text{S37})$$

$$Z_{mn} := l_m^* l_n \langle R_m | R_n \rangle = Z_{nm}^*. \quad (\text{S38})$$

From Eqs. (S36)-(S38), the summation appearing in the second line on the right-hand side of Eq. (S35) can be rewritten as

$$\begin{aligned} \sum_{mn} e^{t\beta_{mn}} Z_{mn} e^{it\alpha_{mn}} &= \sum_m e^{t\beta_{mm}} Z_{mm} + \sum_{m < n} e^{t\beta_{mn}} (Z_{mn} e^{it\alpha_{mn}} + Z_{nm} e^{it\alpha_{nm}}) \\ &= \sum_m e^{t\beta_{mm}} Z_{mm} + 2 \sum_{m < n} e^{t\beta_{mn}} |Z_{mn}| \cos(\theta_{mn} + t\alpha_{mn}). \end{aligned} \quad (\text{S39})$$

Here we have written  $Z_{mn} = |Z_{mn}| e^{i\theta_{mn}}$ . For a  $PT$ -symmetric Hamiltonian  $H$ , we have  $\gamma := \max\{\text{Im}E_m\} \geq 0$ , and hence  $\beta_{\max} := \max\{\beta_{mn}\} = 2\gamma \geq 0$ . Accordingly, we define

$$G(t) := \sum_m e^{-t(\beta_{\max} - \beta_{mm})} Z_{mm} + 2 \sum_{m < n} e^{-t(\beta_{\max} - \beta_{mn})} |Z_{mn}| \cos(\theta_{mn} + t\alpha_{mn}). \quad (\text{S40})$$

With this definition, Eq. (S35) can be rewritten as

$$\text{Im} \langle \psi(t) | H | \psi(t) \rangle = \frac{1}{2} \frac{d}{dt} [e^{t\beta_{\max}} G(t)] = e^{t\beta_{\max}} \left[ \gamma G(t) + \frac{1}{2} G'(t) \right]. \quad (\text{S41})$$

For an initial state  $|\psi(0)\rangle \neq \mathbf{0}$ , we have  $\langle \psi(t) | \psi(t) \rangle = e^{t\beta_{\max}} G(t) > 0$ . Therefore, the loss rate  $L(t)$  is given by

$$\begin{aligned} L(t) &= -2 \text{Im} \langle \tilde{\psi}(t) | H | \tilde{\psi}(t) \rangle \\ &= -2 \frac{\text{Im} \langle \psi(t) | H | \psi(t) \rangle}{\langle \psi(t) | \psi(t) \rangle} = -2\gamma - \frac{G'(t)}{G(t)}. \end{aligned} \quad (\text{S42})$$

For  $\gamma > 0$  and sufficiently large times  $t \gg (\beta_{\max} - \beta_{mn})^{-1}$ , the function  $G(t)$  behaves asymptotically as

$$G(t) \sim \sum_{\substack{m \\ \beta_{mm} = \beta_{\max}}} Z_{mm} + 2 \sum_{\substack{m < n \\ \beta_{mn} = \beta_{\max}}} |Z_{mn}| \cos(\theta_{mn} + t\alpha_{mn}). \quad (\text{S43})$$

As a result,  $L(t)$  oscillates around  $-2\gamma$  (if there exists at least one pair  $m (< n)$  that satisfies  $\beta_{mn} = \beta_{\max}$  and  $\alpha_{mn} \neq 0$ ), or converges to  $-2\gamma$ .

By contrast, when all eigenvalues are real, the restrictions on the summations in Eq. (S43) are lifted, and  $L(t)$  oscillates around zero.

In both cases, since  $\frac{1}{t} \ln[G(t)/G(0)] \rightarrow 0$  as  $t \rightarrow \infty$ , the long-time average satisfies  $\frac{1}{T} \int_0^T dt L(t) \sim -2\gamma$ .

### S3. NEWTON'S IDENTITY

For an arbitrary square matrix  $H \in \mathbb{C}^{n \times n}$ , we define

$$\begin{aligned} P_{\text{inv}}(t) &:= \det[\mathbb{1}_n + tH] \\ &= \prod_{i=1}^n (1 + \lambda_i t) = \sum_{k=0}^n e_k t^k, \end{aligned} \quad (\text{S44})$$

where  $\lambda_i$  ( $i = 1, \dots, n$ ) are the eigenvalues of  $H$  and  $e_k$  ( $k = 1, \dots, n$ ) denote the elementary symmetric polynomials  $e_k = \sum_{1 \leq i_1 < \dots < i_k \leq n} \lambda_{i_1} \cdots \lambda_{i_k}$  with  $e_0 = 1$ .

Let us consider the formal power-series expansion of the logarithm  $\ln P_{\text{inv}}(t)$ :

$$\begin{aligned} \ln P_{\text{inv}}(t) &= \sum_{i=1}^n \ln(1 + \lambda_i t) \\ &= \sum_{i=1}^n \sum_{k=1}^{\infty} \frac{(-1)^{k-1}}{k} (\lambda_i t)^k \\ &= \sum_{k=1}^{\infty} \frac{(-1)^{k-1}}{k} \text{Tr}[H^k] t^k. \end{aligned} \quad (\text{S45})$$

Taking the derivative with respect to  $t$ , we obtain

$$\frac{d}{dt} \ln P_{\text{inv}}(t) = \sum_{k=0}^{\infty} (-1)^k \text{Tr}[H^{k+1}] t^k. \quad (\text{S46})$$

On the other hand, differentiating Eq. (S44) directly yields

$$\frac{d}{dt} P_{\text{inv}}(t) = \sum_{k=0}^{n-1} (k+1) e_{k+1} t^k. \quad (\text{S47})$$

Using the identity  $df/dt = f \cdot d(\ln f)/dt$ , we also have

$$\begin{aligned} \frac{d}{dt} P_{\text{inv}}(t) &= P_{\text{inv}}(t) \frac{d}{dt} \ln P_{\text{inv}}(t) \\ &= \sum_{m=0}^n e_m t^m \sum_{l=0}^{\infty} (-1)^l \text{Tr}[H^{l+1}] t^l \\ &= \sum_{m=0}^n \sum_{l=0}^{\infty} (-1)^l e_m \text{Tr}[H^{l+1}] t^{l+m}. \end{aligned} \quad (\text{S48})$$

By comparing the coefficients of  $t^k$  in Eqs. (S46) and (S48), we obtain

$$\begin{aligned} (k+1)e_{k+1} &= \sum_{0 \leq m \leq n, l \geq 0, l+m=k} (-1)^l e_m \text{Tr}[H^{l+1}] \\ &= \sum_{l=0}^k (-1)^l e_{k-l} \text{Tr}[H^{l+1}]. \end{aligned} \quad (\text{S49})$$

#### S4. CHARACTERIZATION OF $n$ - AND $(n-1)$ -FOLD EPS IN $n$ -BAND SYSTEMS

As mentioned in the main text, a topological invariant allows systematic characterization of EP3s with  $PT$  symmetry for a  $4 \times 4$  matrix. In this section, we explain this fact for  $(n-1)$ -fold EPs described by an  $n \times n$  matrix with/without  $PT$  symmetry. We consider  $n$ - and  $(n-1)$ -fold EPs in an arbitrary  $n$ -band system described by  $H \in \mathbb{C}^{n \times n}$ . To analyze degeneracies of  $H$ , it is convenient to work with the corresponding traceless matrix  $\bar{H} = H - \frac{1}{n} \text{Tr}[H] \mathbf{1}_n$ . The matrix  $\bar{H}$  preserves the symmetries of  $H$  as well as the relative configuration of its eigenvalues. Let  $\lambda_i$  ( $i = 1, \dots, n$ ) be the eigenvalues of  $H$ . Then

$$\begin{aligned} P_{\bar{H}}(E) &:= \det[\bar{H} - E \mathbf{1}_n] \\ &= \prod_{i=1}^n (\bar{\lambda}_i - E) = \sum_{k=0}^n (-1)^k \bar{e}_{n-k} E^k \end{aligned} \quad (\text{S50})$$

holds, where  $\bar{\lambda}_i := \lambda_i - \frac{1}{n} \text{Tr}[H]$ . Here,  $\bar{e}_k$  denotes the  $k$ -th elementary symmetric polynomial of the eigenvalues  $\bar{\lambda}_i$  of  $\bar{H}$ , defined as  $\bar{e}_k := \sum_{1 \leq i_1 < \dots < i_k \leq n} \bar{\lambda}_{i_1} \dots \bar{\lambda}_{i_k}$ , with  $\bar{e}_0 := 1$ . These coefficients can be expressed in terms of the traces  $\text{Tr}[\bar{H}^k]$  via Newton's identities,

$$(k+1)\bar{e}_{k+1} = \sum_{l=0}^k (-1)^l \bar{e}_{k-l} \text{Tr}[\bar{H}^{l+1}], \quad (\text{S51})$$

whose derivation is provided in Sec. S3.

Prior to the characterization of  $(n-1)$ -fold EPs, we discuss  $n$ -fold EPs. If  $H$  has an  $n$ -fold degenerate eigenvalue  $r \in \mathbb{C}$ , all eigenvalues of  $\bar{H}$  must vanish. In this case, the characteristic polynomial of the corresponding traceless matrix  $\bar{H}$  is given by

$$P_{\bar{H}}(E) = (-E)^n. \quad (\text{S52})$$

Since  $\bar{e}_1 = \text{Tr}[\bar{H}] = 0$ , Eqs. (S50) and (S52) imply that, if  $H$  has an  $n$ -fold degenerate eigenvalue  $r \in \mathbb{C}$ , the coefficients  $\bar{e}_k$  vanish for  $k = 2, \dots, n$ . Therefore, imposing these  $n-1$  independent conditions indicates that  $H$  exhibits an EP $n$  with eigenvalue  $r = \frac{1}{n} \text{Tr}[H]$ . This observation also clarifies the codimension of an EP $n$ . In a generic  $n$ -band system, the conditions  $\bar{e}_k = 0$  ( $k = 2, \dots, n$ ) are complex constraints, yielding a codimension  $2(n-1)$ . In contrast, in the presence of  $PT$  symmetry, these coefficients are restricted to be real, so that each condition reduces to a single real constraint. As a result, the codimension is reduced to  $n-1$  under  $PT$  symmetry.

Next, we consider the characterization of  $(n-1)$ -fold EPs. When  $H$  has an  $(n-1)$ -fold degenerate eigenvalue  $r$  and a single eigenvalue  $s$  ( $\neq r$ ), for the corresponding traceless matrix  $\bar{H}$ ,

$$\text{Tr}[H] = (n-1)r + s \Rightarrow \text{Tr}[\bar{H}] = (n-1)\bar{r} + \bar{s} = 0 \quad (\text{S53})$$

and

$$\det[H] = r^{n-1}s \Rightarrow \det[\bar{H}] = (1-n)\bar{r}^n \quad (\text{S54})$$

hold. Here we define  $\bar{r} := r - \frac{1}{n} \text{Tr}[H]$  and  $\bar{s} := s - \frac{1}{n} \text{Tr}[H]$ . Taking these relations into account, we obtain

$$\begin{aligned} P_{\bar{H}}(E) &= (\bar{r} - E)^{n-1}(\bar{s} - E) \\ &= \sum_{k=0}^n (-1)^{n-k} \binom{n}{k} (1-k) \bar{r}^k E^{n-k}. \end{aligned} \quad (\text{S55})$$

Thus, when  $H$  has an  $(n-1)$ -fold eigenvalue  $r$  and a single eigenvalue  $s$  ( $\neq r$ ), each coefficient  $\bar{e}_k$  ( $k = 2, \dots, n-1$ ) satisfies  $\bar{e}_k = \binom{n}{k} (1-k) \bar{r}^k$  [see Eqs. (S50) and (S55)]. Here,  $\bar{r}$  is given by  $\bar{r} = (\det[\bar{H}] / (1-n))^{1/n}$  [see Eq. (S54)]. Combining these relations, we obtain

$$\left( \frac{\bar{e}_k}{\binom{n}{k} (1-k)} \right)^n = \left( \frac{\det[\bar{H}]}{1-n} \right)^k, \quad (\text{S56})$$

for  $k = 2, \dots, n-1$ . Since  $s \neq r$ , it is necessary that  $\det[\bar{H}] \neq 0$ . Therefore, the existence of an  $(n-1)$ -fold EP is confirmed when  $\det[\bar{H}] \neq 0$  and the above  $n-2$  conditions in Eq. (S56) are satisfied. Accordingly, the codimension

of an  $(n-1)$ -fold EP for a generic  $n$ -band system is  $2(n-2)$ , while it is reduced to  $n-2$  in the presence of  $PT$  symmetry. Moreover, the  $(n-1)$ -fold degenerate eigenvalue  $r$  of  $H$  is given by

$$r = \bar{r} + \frac{1}{n} \text{Tr}[H] = \left( \frac{\det[H - \frac{1}{n} \text{Tr}[H] \mathbb{1}_n]}{1-n} \right)^{\frac{1}{n}} + \frac{1}{n} \text{Tr}[H]. \quad (\text{S57})$$

Using the coefficient constraints of the characteristic polynomial in Eq. (S56), we can introduce the coefficient winding number  $W_c$ , in analogy with the resultant winding number  $W_r$ .

For a generic  $n$ -band system with  $n \geq 3$ , an  $(n-1)$ -fold EP is characterized by the vanishing of the following  $2(n-2)$ -dimensional vector:

$$\mathbf{C}(\boldsymbol{\lambda}) = \left( \text{Re } c_1, \text{Im } c_1, \dots, \text{Re } c_{n-2}, \text{Im } c_{n-2} \right)^T. \quad (\text{S58})$$

Here, each component  $c_k(\boldsymbol{\lambda})$  ( $k = 1, \dots, n-2$ ) is defined as

$$c_k(\boldsymbol{\lambda}) = \left( \frac{\bar{e}_{k+1}(\boldsymbol{\lambda})}{\binom{n}{k+1}(-k)} \right)^n - \left( \frac{\det[\bar{H}(\boldsymbol{\lambda})]}{1-n} \right)^{k+1}. \quad (\text{S59})$$

Let  $\boldsymbol{\lambda}_0 \in X$  denote a parameter point corresponding to an  $(n-1)$ -fold EP in  $2(n-2)$ -dimensional parameter space  $X$ . For parameter points  $\mathbf{p} \in S^{2(n-2)-1} \subset X \setminus \{\boldsymbol{\lambda}_0\}$  surrounding  $\boldsymbol{\lambda}_0$ , one can introduce a mapping between  $(2n-5)$ -spheres,  $\mathbf{n} = \mathbf{C}/\|\mathbf{C}\| : S^{2n-5} \rightarrow S^{2n-5}$ . The homotopy class of this mapping is characterized by  $\pi_{2n-5}(S^{2n-5}) = \mathbb{Z}$  and thus takes integer values, which are given by the winding number

$$W_c = \frac{\epsilon^{i_1 \dots i_{2n-5}}}{2\pi^{n-2}/(n-3)!} \int d^{2n-5} \mathbf{p} f_{i_1 \dots i_{2n-5}}. \quad (\text{S60})$$

Here,  $\epsilon^{i_1 \dots i_{2n-5}}$  is the totally antisymmetric tensor satisfying  $\epsilon^{12 \dots (2n-5)} = 1$ , and  $f_{i_1 \dots i_{2n-5}} = n_{i_1} \partial_1 n_{i_2} \partial_2 n_{i_3} \dots \partial_{2n-5} n_{2n-4}$ .

Moreover, for an  $(n-1)$ -fold EP at  $\boldsymbol{\lambda} = \boldsymbol{\lambda}_0$  in  $(n-2)$ -dimensional parameter space  $X'$  protected by  $PT$  symmetry, an  $(n-2)$ -component vector  $\mathbf{C}(\boldsymbol{\lambda}) = (c_1(\boldsymbol{\lambda}), \dots, c_{n-2}(\boldsymbol{\lambda}))^T$  vanishes. Therefore, for parameter points  $\mathbf{p} \in S^{n-3} \subset X' \setminus \{\boldsymbol{\lambda}_0\}$  surrounding  $\boldsymbol{\lambda}_0$ , one can introduce a mapping between  $(n-3)$ -spheres,  $\mathbf{n} = \mathbf{C}/\|\mathbf{C}\| : S^{n-3} \rightarrow S^{n-3}$ , from which the winding number

$$W_c = \frac{\epsilon^{i_1 \dots i_{n-3}}}{A_{n-3}} \int d^{n-3} \mathbf{p} f_{i_1 \dots i_{n-3}} \quad (\text{S61})$$

is obtained. Here, for a nonnegative integer  $m$ ,

$$A_{n-3} = \begin{cases} 2\pi^{m+1}/m! & (n = 2(m+2)), \\ 2^{2m+1}\pi^m m!/(2m)! & (n = 2m+3), \end{cases} \quad (\text{S62})$$

which corresponds to the surface area of the  $(n-3)$ -dimensional unit sphere.

## S5. NUMERICAL DATA FOR THE BOSONIC TOY MODEL

In the main text, we demonstrated the emergence of interaction-enabled EL2s using the topological index  $s_{(2,+)}(\boldsymbol{\lambda})$ , defined as  $s_{(2,+)}(\boldsymbol{\lambda}) = \text{sgn}(\text{Disc}[\det[H_{(2,+)}(\boldsymbol{\lambda})]])$ . For clarity, we rewrite  $H_{(2,+)}(\boldsymbol{\lambda})$  explicitly as

$$\begin{aligned} H_{(2,+)}(x, y) &= \begin{pmatrix} H_{0(2,+1)}(x, y) & \\ & H_{0(2,+,-1)}(x, y) \end{pmatrix} + H_{\text{int}(2,+)} \\ &= w \mathbb{1}_4 + \begin{pmatrix} x - i\delta & y & & \\ y & -x + i\delta & & \\ & & -x - i\delta & y \\ & & y & x + i\delta \end{pmatrix} + \begin{pmatrix} V & U & & \\ U & V & & \\ & & U & V \end{pmatrix}, \end{aligned} \quad (\text{S63})$$

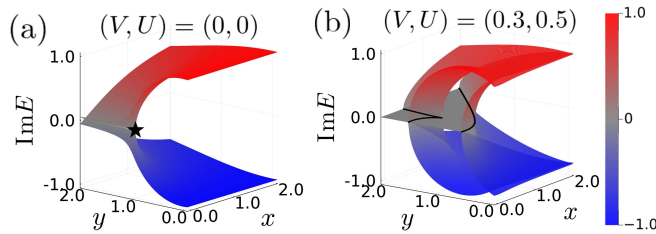


FIG. S1. (a) [(b)]:  $x$ - $y$  dependence of the imaginary parts of the complex eigenvalues of  $H_{(2,+)}$  for  $(w, \delta) = (0, 1)$  with  $V = U = 0$  [ $(V, U) = (0.3, 0.5)$ ]. In panel (a), the black star at  $(x, y) = (0, \delta)$  represents an EP2, whereas in panel (b), black lines represent EL2s.

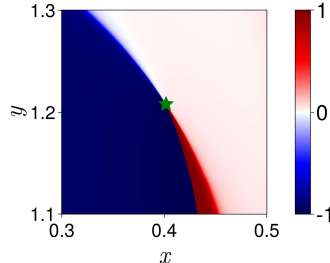


FIG. S2.  $x$ - $y$  dependence of the principal value of the argument of  $Z_c$  divided by  $\pi$  for  $(w, \delta, V, U) = (0, 1, 0.3, 0.5)$ . The green stars indicate  $\lambda_{EP3} \sim (0.402, 1.208)$ .

where omitted entries are zero. Figure S1 shows the  $x$ - $y$  dependence of the imaginary parts of the complex eigenvalues of  $H_{(2,+)}(\lambda)$ . As shown in Fig. S1(a), in the absence of interactions, no one-dimensional regions of degenerate eigenvalues appear. In contrast, as shown in Fig. S1(b), the presence of interactions gives rise to one-dimensional regions, indicated by the black lines, where the imaginary parts of the eigenvalues become degenerate. In these regions, the real parts of the eigenvalues are simultaneously degenerate. These results provide a direct visualization of the emergence of interaction-enabled EL2s.

In Fig. S1(b), one can find a cusp structure of the interaction-enabled EL2 which corresponds to the interaction-enabled EP3 discussed in the main text. While the resultant winding number can characterize the interaction-enabled EP3, we characterize it using an alternative topological invariant  $W_c$  introduced in Sec. S4. Since  $H_{(2,+)}(\lambda)$  is a  $PT$ -symmetric four-band model, a topological invariant for the interaction-enabled EP3s can be introduced as

$$W_c = \oint \frac{d\lambda}{2\pi i} \cdot \partial_\lambda \ln Z_c(\lambda), \quad (S64)$$

where  $Z_c(\lambda) = c_1(\lambda) + i c_2(\lambda)$ , and  $c_k(\lambda)$  ( $k = 1, 2$ ) are defined in Eq. (S59). This invariant  $W_c$  is equivalent to setting  $n = 4$  in Eq. (S61). Figure S2 shows the  $x$ - $y$  dependence of the principal value of the argument of  $Z_c$ . When the parameters encircle  $\lambda_{EP3}$  counterclockwise, we obtain the winding number  $W_c = -1$ . Namely, the zeros of  $C(\lambda) = (c_1(\lambda), c_2(\lambda))^T$  enable the detection of interaction-enabled EP3s of  $H_{(2,+)}(\lambda)$  over the entire two-dimensional parameter space, independent of the choice of  $E_{EP3}$ .

## S6. INTERACTION-ENABLED EL2S AND EP3S IN FERMIONIC SYSTEMS

In the main text, we have revealed the existence of interaction-enabled EL2s and EP3s in bosonic systems. Our framework can be applied to fermionic systems as well. In this section, we show, using a toy model, that interaction-enabled EL2s and EP3s also emerge in fermionic systems with charge  $U(1)$ , pseudo-spin-parity, and  $PT$  symmetries.

We consider a two-component fermionic toy model:

$$\hat{H}(x, y) = \hat{H}_{0A}(x, y) + \hat{H}_{0B}(x, y) + \hat{H}_{int}, \quad (S65)$$

$$\hat{H}_{0\tau} = \hat{\Psi}_{f,\tau}^\dagger h_\tau(x, y) \hat{\Psi}_{f,\tau} \quad (\tau = A, B), \quad (S66)$$

$$\hat{H}_{int} = V \sum_{i=1}^3 (\hat{f}_{i,A}^\dagger \hat{f}_{i,B} \hat{f}_{i+1,A}^\dagger \hat{f}_{i+1,B} + \text{h.c.}), \quad (S67)$$

where real parameters  $x$  and  $y$  describe a two-dimensional parameter space. Here,  $\hat{\Psi}_{f,\tau}^\dagger = (\hat{f}_{1,\tau}^\dagger, \hat{f}_{2,\tau}^\dagger, \hat{f}_{3,\tau}^\dagger)$ , where  $\hat{f}_{i,\tau}^\dagger$  ( $\hat{f}_{i,\tau}$ ) is the creation (annihilation) operator of a fermion with component  $\tau$  ( $= A, B$ ) on site  $i$  ( $= 1, 2, 3$ ). In the interaction term,  $V$  is a real parameter representing the interaction strength, and we identify  $i + 1 := 1$  when  $i = 3$ . The first-quantized Hamiltonian  $h_\tau(x, y)$  is given by

$$h_\tau(x, y) = \begin{pmatrix} (-1)^{\delta_{B,\tau}} x - i\delta & y & y \\ y & 0 & y \\ y & y & -(-1)^{\delta_{B,\tau}} x + i\delta \end{pmatrix}. \quad (\text{S68})$$

$\hat{H}(x, y)$  preserves charge U(1), pseudo-spin-parity, and  $PT$  symmetries [Eqs. (S1)–(S3)]. The  $PT$  operator is defined as

$$\hat{P}\hat{T} = \exp \left[ i \frac{\pi}{2} \sum_{i,j} (p_{ij} \hat{f}_{i,A}^\dagger \hat{f}_{j,B} + p_{ij}^T \hat{f}_{i,B}^\dagger \hat{f}_{j,A}) \right] \mathcal{K}, \quad (\text{S69})$$

where  $p = \begin{pmatrix} 0 & 0 & 1 \\ 0 & 1 & 0 \\ 1 & 0 & 0 \end{pmatrix}$  and  $\mathcal{K}$  denotes the complex conjugation operator.

We focus on the Fock-space sector with  $(N, (-1)^{N_B}) = (2, +)$ , satisfying  $N + 1 + \sigma = 0 \pmod{4}$ . The Hamiltonian  $H_{(2,+)}$  which acts closely within this subspace is given by,

$$H_{(2,+)} = \begin{pmatrix} H_{0(2,+,T_z=+1)} & O \\ O & H_{0(2,+,T_z=-1)} \end{pmatrix} + V \begin{pmatrix} O & \mathbb{1}_3 \\ \mathbb{1}_3 & O \end{pmatrix}, \quad (\text{S70})$$

$$H_{0(2,+,T_z)} = \begin{pmatrix} (-1)^{\delta_{T_z,-1}} x - i\delta & -y & -y \\ -y & i\delta - (-1)^{\delta_{T_z,-1}} x & -y \\ -y & -y & 0 \end{pmatrix}. \quad (\text{S71})$$

The basis is chosen as

$$(|A1, A2\rangle, |A2, A3\rangle, |A3, A1\rangle, |B1, B2\rangle, |B2, B3\rangle, |B3, B1\rangle), \quad (\text{S72})$$

where the basis states are defined as  $|\tau i, \tau j\rangle = \hat{f}_{i,\tau}^\dagger \hat{f}_{j,\tau}^\dagger |0\rangle$ . Since the relations  $H_{(2,+)}(-x, y) = S H_{(2,+)}(x, y) S^{-1}$  with  $S = \tau_1 \otimes \mathbb{1}_3$  and  $H_{(2,+)}(x, -y) = -R \mathcal{K} H_{(2,+)}(x, y) (R \mathcal{K})^{-1}$  with  $R = \tau_2 \otimes \mathbb{1}_3$  hold, we focus our analysis on the first quadrant of the  $x$ - $y$  plane.

We choose  $y = 1$  as an illustrative example and plot the  $x$ -dependence of the complex eigenvalues of  $H_{(2,+)}(x, y = 1.0)$  in Fig. S3(a). In contrast to the case for  $V = 0$ , both the real and imaginary parts of the eigenvalues become degenerate at  $y \sim 0.41$  and  $y \sim 1.25$  for  $V = 1$ , indicating the emergence of interaction-enabled EP2s. Correspondingly, the  $\mathbb{Z}_2$  index  $s_{(2,+)}(x, y = 1.0)$  jumps at these EP2s [see Fig. S3(b)], characterizing their topology. Moreover, Fig. S3(b) shows that these EP2s extend to other values of  $y$ , indicating the emergence of interaction-enabled EL2s in the  $x$ - $y$  plane (see also Fig. S4).

Furthermore, the two cusps on the interaction-enabled EL2s observed in Fig. S3(b) at  $\lambda_1 \sim (0.071, 0.669)$  and  $\lambda_2 \sim (0.315, 0.057)$  are identified as interaction-enabled EP3s with  $\mathbb{Z}$  topology through the resultant winding number.

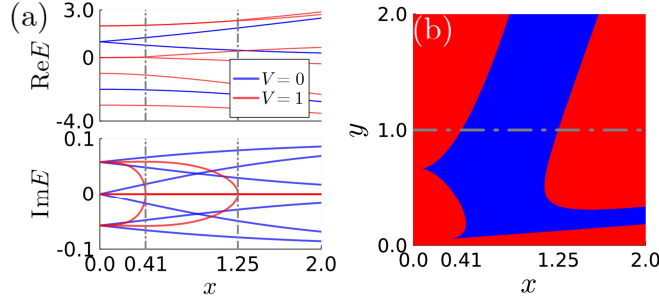


FIG. S3. (a):  $x$ -dependence of the eigenvalues of  $H_{(2,+)}(x, y = 1)$  for  $\delta = 0.1$ . The blue and red solid lines correspond to  $V = 0$  and  $V = 1$ , respectively. (b): The  $\mathbb{Z}_2$  topological index  $s_{(2,+)}(x, y)$  for  $\delta = 0.1$  and  $V = 1$ . The blue and red regions correspond to  $s = -1$  and  $s = +1$ , respectively.

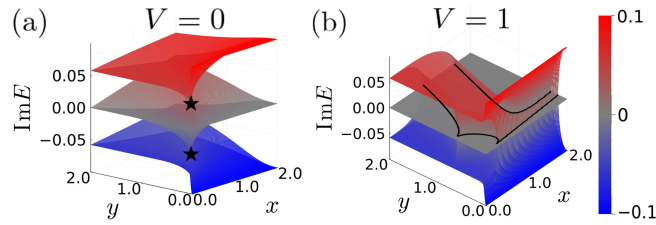


FIG. S4. (a) [(b)]:  $x$ - $y$  dependence of the imaginary parts of the complex eigenvalues of  $H_{(2,+)}$  for  $\delta = 0.1$  with  $V = 0$  [ $V = 1$ ]. In panel (a), the black stars at  $(x, y, \text{Im}E) = \delta(\sqrt{7 - 4\sqrt{3}}, \frac{2}{3}\sqrt{2\sqrt{3} - 3}, \pm \frac{\sqrt{3}}{3}\sqrt{2\sqrt{3} - 3})$  each represent an EP2, whereas in panel (b), black lines represent EL2s.

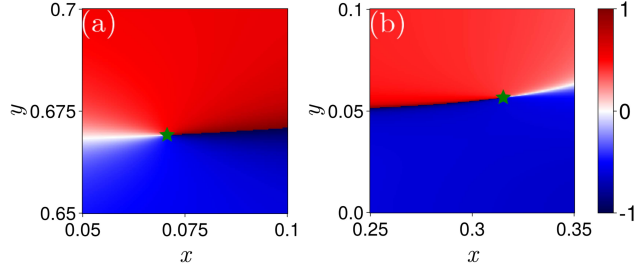


FIG. S5. (a) [(b)]:  $x$ - $y$  dependence of the principal value of  $Z_r$  for  $(\delta, V) = (0.1, 1)$  with  $E_{\text{ref},1} \sim -1.033$  [ $E_{\text{ref},2} \sim -0.331$ ] divided by  $\pi$ . The green star indicates  $\lambda_1 \sim (0.071, 0.669)$  [ $\lambda_2 \sim (0.315, 0.057)$ ].

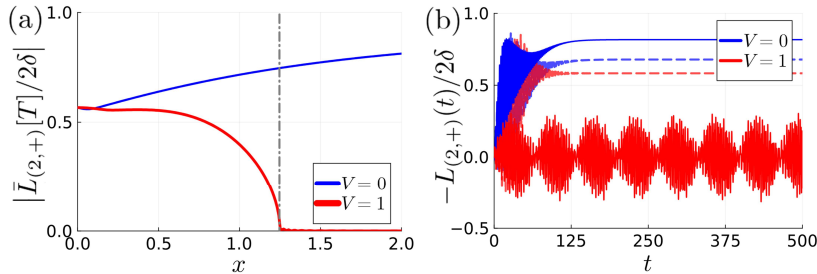


FIG. S6. (a): Dependence of  $|\bar{L}_{(2,+)}[T]/2\delta|$  on  $x$  for  $(\delta, y, T) = (0.1, 1.0, 500)$ . The gray dashed line indicates  $y = 1.25$ . (b): Time dependence of  $-L_{(2,+)}(t)/2\delta$  for  $(\delta, y) = (0.1, 1.0)$ . The dashed and solid lines correspond to  $x = 0.5$  and  $x = 1.5$ , respectively. In panels (a) and (b), blue and red denote the cases  $V = 0$  and  $V = 1$ , respectively.

Indeed, when the parameters  $(x, y)$  encircle the cusps  $\lambda_1$  and  $\lambda_2$  counterclockwise, the resultant winding number takes the values  $-1$  and  $+1$ , respectively (see Fig. S5).

The existence of interaction-enabled EL2s protected by  $PT$  symmetry is also reflected in the behavior of the loss rate in fermionic systems. We set the initial state as  $|\psi(0)\rangle = \frac{1}{\sqrt{2}}(|A_2, A_3\rangle + |B_1, B_2\rangle)$  and discuss the behavior of the loss rate at  $y = 1$ , the same value as in Fig. S3(a). Figure S6(a) shows that the time-averaged loss rate  $\bar{L}_{(2,+)}[T]$  rapidly approaches zero in the vicinity of the interaction-enabled EP2 located at  $x \sim 1.25$ , following the  $x$  dependence of the maximum imaginary part of the complex eigenvalues, and becomes  $\bar{L}_{(2,+)}[T] \sim 0$  for  $x \gtrsim 1.25$ . In addition, Fig. S6(b) shows that the presence of interaction-enabled EL2s is also reflected in the time-dependence of the loss rate.